NATIONAL AERONAUTICS AND SPACE ADMINISTRATION

Technical Report 32-1280

Experimental Studies with a Mercury Bombardment Thrustor System

Tommy D. Masek

JET PROPULSION LABORATORY
CALIFORNIA INSTITUTE OF TECHNOLOGY
PASADENA, CALIFORNIA

July 15, 1968

NATIONAL AERONAUTICS AND SPACE ADMINISTRATION

Technical Report 32-1280

Experimental Studies with a Mercury Bombardment Thrustor System

Tommy D. Masek

Approved by:

D. R. Bartz, *Manager*
Research and Advanced Concepts Section

JET PROPULSION LABORATORY
CALIFORNIA INSTITUTE OF TECHNOLOGY
PASADENA, CALIFORNIA

July 15, 1968

TECHNICAL REPORT 32-1280

Prepared Under Contract No. NAS 7-100
National Aeronautics & Space Administration

Contents

Tables

Contents (contd)

Figures

Acknowledgment

The author gratefully acknowledges the assistance of the Applications Studies Laboratory personnel, particularly Roy W. Adams for preparing the laboratory power and instrumentation systems used in testing, and Elwood Hooper for cluster assembly. In addition, the design and drafting work of Gerrit Steenhagen and the helpful suggestions and support of Eugene V. Pawlik, Daniel J. Kerrisk, and J. R. Womack are credited.

Abstract

Tests performed with a mercury-electron-bombardment ion engine system are discussed in this paper. The total assembly is composed of four 2.5-kW thrustors, individual isolated feed systems, and two 200-lb capacity propellant tankage systems. The thrustors, nominally 20 cm in diam, utilize a reverse-feed propellant introduction method, electromagnets, and oxide cathodes. The propellant tankage uses a neoprene bladder expulsion method pressurized by Freon. Preliminary tests showed that all components operated satisfactorily and a system power-to-thrust ratio of about 120 kW/lb was achieved at about 3500 s, specific impulse. These experiments show that with modest optimization, a basic propulsion system design will be available for advanced system development.

Experimental Studies with a Mercury Bombardment Thrustor System

I. Introduction

Interplanetary missions using solar-powered electric propulsion have been under investigation (Refs. 1–3) for the past three years. These investigations have shown that, if the existing electric propulsion component technology were applied, missions with improvements over chemical propulsion systems could be accomplished. Although the component technology appears to be sufficiently developed for spacecraft application, the existence of a system technology remains to be demonstrated.

The electric propulsion system is composed of the power subsystem and the thrust subsystem. The former is presently being developed under contract (Ref. 4); the latter is the subject of this report.

Consideration of spacecraft propulsion system functional requirements has identified the following elements of the thrust subsystem (Ref. 5): (1) thrustors, (2) propellant tankage, (3) power conditioning and controls, (4) load matching and switching, and (5) thrust-vector position control. A relatively well-developed technology exists for the first three elements, but the remaining two are essentially undeveloped. In order to demonstrate the capabilities of electric propulsion realistically, the major subsystems must be developed and tested in a system configuration.

Propulsion system weight, efficiency, and reliability requirements are highly mission dependent (Refs. 1–3). However, conservative estimates of these requirements can be established (Ref. 5) based on the most stringent conditions. The estimates of Ref. 5 will be used as performance goals for the propulsion system development program. These goals are: (1) a propulsion system weight (exclusive of solar panels) of 20 lb/kW of electric power from the solar panels at 1 AU, (2) a total efficiency (thrust power to solar panel power) of 60% or a power-to-thrust ratio of 127 kW/lb at 3500 s true specific impulse, and (3) a total system reliability of at least 95% for a 10,000-h life.

The power conditioning and load matching systems can only be specified after a firm design has been established for the thrustor and propellant tankage systems. Therefore, the first steps in a propulsion system technology program are: build the thrustor and tankage systems; develop power and control requirements. Since the mission profiles so far considered require the thrustor system

to operate over some power range, both the thrustor's performance at its nominal design point, and its off-design capabilities are needed.

This paper presents the initial results of an experimental program to produce an integrated propulsion system, but deals primarily with the thrustor and propellant tankage. The assembly, consisting of an array of four thrustors and two propellant tanks, will be initially used to establish reasonable thrustor and tankage designs. The off-design capabilities will then be tested to provide information for power matching and to develop power conditioning and control requirements.

The present study concerns both the design philosophy and the hardware. Previous investigations at NASA-Lewis (Refs. 6–8) have covered the problems associated with clustering, but did not include many of the problems related to spacecraft, such as thrustor packaging and multiple isolated propellant systems. The present study answers some of these questions, provides a good starting point for the complete propulsion system design, and describes the first ten runs of the system.

II. Thrustor and Propellant Tankage Systems Design

A. Design Criteria

In order to design and build a propulsion system representative of solar electric propulsion technology, and yet avoid the lure of searching for higher performance through extensive research, design criteria and constraints were established. These were selected largely by resource limitations and the present state of the art. It was immediately recognized that any system built using present technology would probably be substantially out of date within a few years (i.e., the time required for its design and testing). Therefore, the basic guidelines for the investigation described in this paper were: (1) to establish a system design containing the basic elements presently thought to be required for a spacecraft application, and (2) to operate this system in a mode duplicating that required by a solar electric spacecraft. More detailed criteria follow directly from these guidelines.

A number of the constraints placed on the present thrustor and propellant tankage subsystems designs were based on recent mission studies. These studies of several missions with different flight times, power levels, and spacecraft sizes, were used to establish system requirements common to a number of possible missions. The flight times expected for the missions of current interest vary widely (Refs. 1, 2). However, thrusting times appear to be similar and are on the order of one year. Thus, a representative operating time of 10,000 h was established for the present study. Power levels from 5 to 20 kW are of interest for near-future missions with existing *Atlas-Centaur* or *Titan III* launch vehicles (Refs. 1–3). Power levels to 70 kW would be of interest for *Saturn*-class vehicles. Since most interest centers on possible early applications with available boosters, a power level of 10 kW was chosen for the system. Test facility constraints as well as resource limitations also set 10 kW as an upper limit.

A major factor in choosing a propulsion system concept is reliability. Extensive studies of reliability indicate that a modular approach in all components is desirable (Refs. 1, 2). This approach is particularly important for solar electric systems because the available solar power changes throughout the mission. This requires the thrustor system to operate over a wide power range. Individual thrustors, however, operate efficiently only over a narrow power range off the design point ($\pm 20\%$). The modular system allows thrustors to be shut off or started as required to utilize full solar power and still operate efficiently. The spare thrustors and their support systems, either at the beginning or the end of the flight, are then available to replace systems that possibly failed.

An individual thrustor power level of 2.5 kW was selected for this work. This level was chosen because of its applicability to missions currently being investigated (Refs. 9, 10). Four 2.5-kW thrustors also represent a reasonable demonstration of the modular design approach. Current detailed mission analyses (Refs. 9, 10) indicate that the specific impulse range of interest is between 2,500 and 4,000 s. Although higher I_{sp}'s can generally be achieved with thrustors designed for low I_{sp}, the reverse is not true. Thus, a portion of the present work is devoted to electrode design for the low I_{sp} range. As noted previously, the primary purpose of the present solar electric program is to integrate the various subsystems into a working propulsion system. The initial design performance goal for these systems was optimistically set at a power-to-thrust ratio of 130 kW/lb at an I_{sp} of 3500 s.

In addition to performance and reliability, system weight is of great importance. As indicated previously, a goal of 20 lb/kW has been established for the demonstration propulsion system. Of this, a maximum of 10 lb/kW is estimated for the power conditioning and load matching systems. The weight goal of the present

system, including thrustor and propellant tankage subsystems, wiring, and structure, is 10 lb/kW. The wiring and structure are expected to be representative of those required in the final propulsion system. In this case the "structure" will be replaced by the thrust-vector tracking system.

With the foregoing design criteria in mind, the basic thrustor and propellant tankage system was selected to have the form shown schematically in Fig. 1. As shown in Fig. 1, two propellant tankage assemblies were selected. This was done to simplify packaging and reduce propellant handling and assembly for laboratory tests. The propellant tanks feed a manifold common to the four thrustors. Individual vaporizers feed the vaporized propellant through isolators used to electrically isolate the thrustor and propellant systems. A "reverse feed" type propellant supply system (Ref. 11), in which propellant enters from the side and is directed rearward, is also shown. Ion-beam neutralizers are included for individual engines, although it may be possible to reduce this number. A more detailed description of the present component and system design is given in the next sections.

B. Component Design

The component design was guided principally by two factors: (1) flexibility, and (2) use of current state-of-the-art technology. This required that a number of choices be made in order to use the immediately available technology and eliminate time-consuming development. These

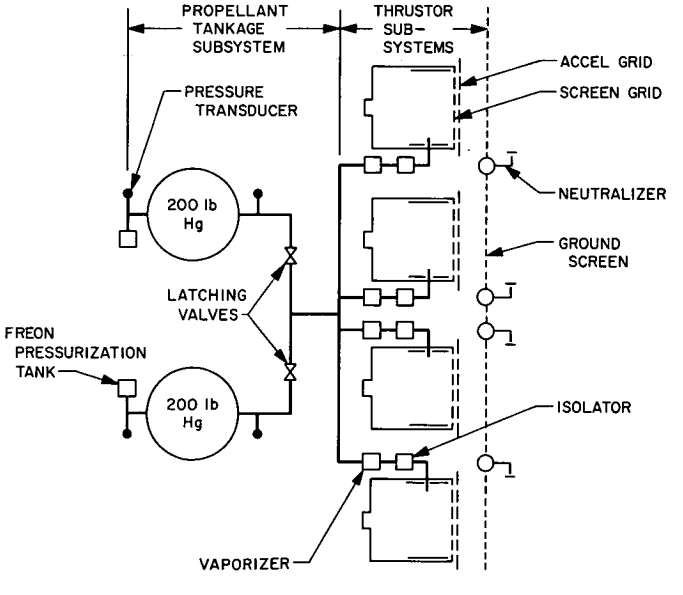

Fig. 1. Clustered ion engine system, schematic diagram

choices centered on the following areas: (1) magnets, (2) cathodes, and (3) neutralizers.

Both electromagnet and permanent-magnet thrustors have been tested extensively (Refs. 12, 13). Electromagnets have the advantages of adjustability and complete shutoff. They have the disadvantage of requiring a power supply. Permanent magnets eliminate the need for a power supply, but reduce thrustor control and cannot be shut off. Magnetic-field interactions with spacecraft measurements may dictate the use of electromagnets. Electromagnets were chosen in the present work to allow performance mapping and optimization and to avoid the spacecraft interaction problem. Permanent magnets could be substituted later by eliminating the magnet circuit of the power conditioning system, whereas the reverse situation is not true.

Cathode development has also continued for several years. The hollow cathode being developed for SERT II, appears to hold the greatest lifetime possibilities (Ref. 4). The major difficulty in using this cathode is in off-design operation, since a critically controlled mercury flow is required for operation. If operated with a separate mercury supply system, the hollow cathode should prove quite useful. However, this cathode is presently unavailable in the size required for a 2.5-kW thrustor. An oxide cathode of the Hughes spiral type (Ref. 2) has been adopted in this work, pending the development of the hollow cathode.

The Electro-Optical Systems cesium-plasma bridge neutralizer (Ref. 14) was selected because of its availability. The mercury-plasma bridge neutralizer (Ref. 15) should work equally well, but was not immediately available at the time. Using the previous design criteria and characteristics, the details of the present design will now be outlined.

C. Thrustor Subsystem

The thrustor used in this investigation is shown in Fig. 2. The power level of 2.5-kW total was determined, as indicated previously, by the choice of a four-module, 10-kW array. A nominal 20-cm-diam thrustor was selected by extrapolation from smaller thrustors and previous 20-cm thrustor tests at NASA-Lewis (Ref. 8). At a specific impulse of about 3500 s, a mass-utilization efficiency of 85%, and a power efficiency of 70%, a beam current of approximately 1 A is required. These conditions, together with the requirement of an accel-decel ratio of about 2 for good beam focusing, indicate that spacing of 0.060

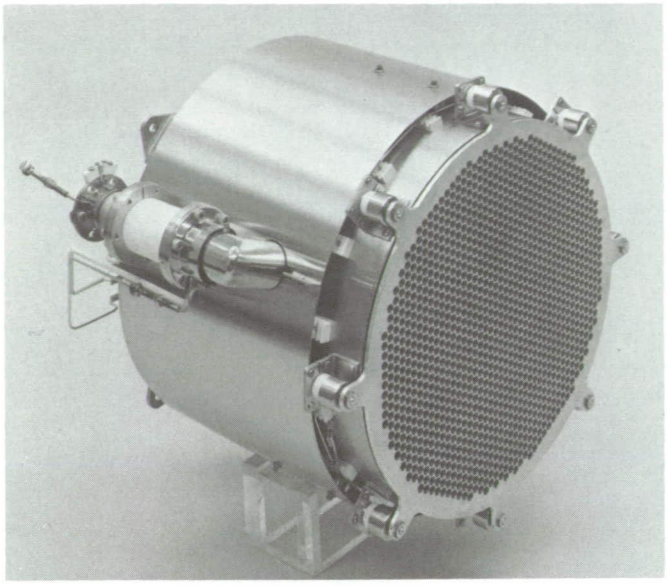

Fig. 2. The 20-cm ion engine thrustor

to 0.070 in. is required between the screen grid and the accel grid.

The grid-aperture diameter of 0.187 in. was chosen initially. A total of 1385 apertures were used, giving an open area of 245 cm^2, or about 75% open area. Thus, for a beam current of 1 A, the average current density is about 4 mA/cm^2. Grids with smaller apertures will be investigated, but are not included in this report. The screen grids were chamfered conventionally on the plasma side. All grids were nominally 0.100 in. thick and were fabricated from molybdenum (TZM).

The accel-grid support structure (Fig. 2) used standard alumina insulators mounted to small brackets attached to the housing. Grid alignment and positioning was accomplished with this system through two locking nuts on each support. Prerun screen-accel aperture alignment and grid-spacing tolerances of ± 0.001 in. were obtained with this method.

The thrustor had a length-to-diam ratio of unity, based on anode diam and all metallic parts were stainless steel. The 0.030-in.-thick housing was supported by internal rings screwed in place. Six insulators, similar to the grid-support insulators, were used to mount the 8-in.-diam, 4-in.-long anode. The mounting position was 0.37 in. from the screen grid and 0.25 in. from the housing.

In the basic design, propellant enters the thrustor approximately 2.5 in. from the screen grid. The feed line is attached to the housing but passes through the anode. Propellant is distributed from a slot and is directed generally toward the cathode. A distribution manifold was not used because of pressure requirements of the isolator. Tests with propellant injected through the rear of the engine are discussed in a later section.

1. Isolator. Electrical isolation of the thrustor and propellant tankage systems is an important part of the present system concept. Isolation allows a common propellant system to be used without the problem of electrically coupled thrustors. The isolator was designed to operate below 0.3 torr/cm based on the mercury Paschen curve (Ref. 16). Flowrate calculations (Ref. 17) indicated that a pressure of about 0.05 torr would exist in the isolator for a flowrate of 10 g/h, using the 2.5-cm-diam feed-line configuration shown in Fig. 2. Thus, an isolator 5 cm long, 2.5 cm in diam, was established to maintain a breakdown voltage of at least 5 kV. Boron nitride was used for initial isolator tests because of fabrication ease and previous successful operation. Because of its strength and brazing advantages, Lucalox (high density alumina) will be used after the isolator design has been verified. Split ring clamps, fitting against flanges machined on the isolator, were used for mounting. A flat 20-mesh screen was used to provide a plasma boundary at the thrustor end of the isolator.

2. Vaporizer. Vaporization of the liquid mercury was accomplished by means of a heated, porous tungsten disk. It is desirable to maintain the liquid-vapor interface at the upstream vaporizer surface to maintain liquid control and vaporization stability (Ref. 18). Tungsten was chosen, rather than stainless steel, because mercury was previously found to wet stainless after several hundred hours of operation. In order to maintain flexibility in the vaporizer design, the tungsten disk was electron-beam-welded to a removable molybdenum assembly. The tungsten disk was 0.5 in. in diam and 0.060 in. thick. An average pore size of 8 μ (2 to 24 μ) and a density of 70% of theoretical was chosen (Philips Metalonics, Mod. A). This choice was based on calculations using an empirical formula for flow through porous beds (Ref. 19). These calculations did not predict the correct flowrate variation with temperature compared to calibrations, but did predict the correct order of magnitude at reasonable temperatures.

A bell-jar calibration of four vaporizer assemblies showed the flowrate vs temperature curves to be self-consistent and to have variations of less than 10%. However, tests with the cluster proved this calibration to be

too low, resulting in an uncertainty in mass utilization efficiency. Because of this uncertainty and the importance of accurate mass utilization efficiency measurements in evaluating total efficiency, an externally controlled mercury supply system was established. The mercury was fed to the vaporizers from standard 1-ml pipettes from which an accurate measurement of the mercury level could be obtained. With this method, flowrate measurements accurate to about ±1% could be obtained in a period of 30 min. The measurements were found to depend on the elimination of all air bubbles in the feed lines. Several tests were performed to show repeatability and the lack of liquid level change when the pipettes were pressurized to about 5 psig. The vaporizers were calibrated as a function of temperature in this way during operation. This calibration is of importance only for laboratory operation, since the presently proposed control system will control the vaporizer from the beam current. Additional bell-jar tests showed that a pressure difference across the tungsten disk of 50 psi was required to force liquid through the disk. This value set the upper limit of pressurization in the propellant tankage system.

3. Neutralizer. To simplify testing, neutralizers were not installed during the preliminary tests. These have been provided for in the system design and will be used in later tests.

D. Propellant Tankage Subsystem

Propellant requirements were determined from the previous design criteria. Since a changing power level is expected for a solar-powered flight, the propellant flowrate required will also change. It was estimated that only about one half the propellant needed for a constant-power, 10-kW, 10,000-h mission would be required for a typical solar electric mission. Thus, two tanks with 200-lb capacity each were selected. A positive expulsion-type tank design was developed utilizing a hemispherical neoprene bladder. The pressurization system was formed by attaching a small reservoir of liquid Freon 113 on the gas side of the bladder. The mercury side of each tank was connected to a common manifold through valves. A neoprene bladder was used to satisfy compatibility requirements with mercury and Freon 113. Tests were performed to verify mercury compatibility by submerging stretched neoprene samples in a pan of mercury for 2800 h. Results of this test are shown in Table 1. No sample failures occurred and after initial stretching no further change in elongation occurred during the test period.

Table 1. Neoprene compatibility tests

Sample	Initial elongation, % (based on 2.00 in.)	Permanent elongation, % after 2800 h
1	13	5
2	27	9
3	51	14

To check the permeability of neoprene to Freon 113, a rough test was performed. A 0.060-in.-thick neoprene sheet was clamped to a 3-in.-diam hemisphere. A 1-ml pipette was filled with Freon and attached to the hemisphere. At room temperature the Freon evaporated slowly from the pipette to establish an equilibrium partial pressure in the hemisphere. After about 800 h the Freon had evaporated from the pipette, although the hemisphere was pressurized, as indicated by an outward deflection of the neoprene sheet. A halogen detector was used to test for leakage, but no Freon was detected. The hemisphere was still pressurized after about 4000 h, indicating that the Freon-neoprene combination is suitable.

The propellant tankage design used in this work is shown in Fig. 3. The 0.060-in.-thick bladder forms an O-ring seal between the hemispheres and has 0.030-in. ridges on the mercury side to avoid trapping liquid against the tank. The hemispheres are clamped together at the present time to allow easy disassembly in checking the design. However, in the lightweight stainless-steel version successfully fabricated, the hemispheres were joined by electron-beam welding. In addition, a tankage assembly has been fabricated from 6A1-4V titanium. Tank wall thicknesses of 0.040 in. were used in the present study.

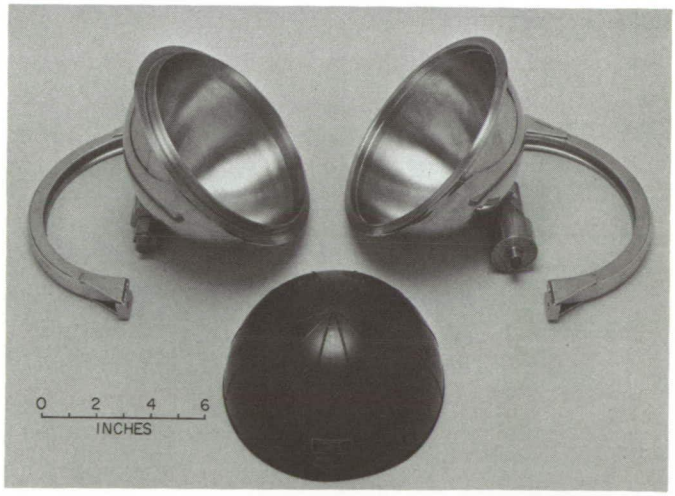

Fig. 3. Zero-gravity propellant tankage subsystem

The Freon-pressurization system is composed of a 2-in.-diam, 5-in.^{3} cylinder connected to a small check valve. Upon assembly, the ball of the check valve is depressed, allowing the Freon to flow to the propellant tank. The Freon storage will be made integral with the propellant tank, once the liquid Freon requirement is confirmed. The pressure supplied by the Freon 113 depends on the tankage temperature. It is expected that a spacecraft utilizing electric propulsion would have some form of thermal control. Thus, a system capable of working within reasonable temperature limits will be satisfactory. The present system will perform adequately between 60° and 180°F. The lower temperature represents the pressure required to exceed the vapor pressure of mercury at the vaporizer (about 5 psia), while the higher temperature corresponds to the pressure limit of the vaporizer (50 psia) to retain liquid.

Pressure transducers were included on both Freon and mercury halves of the propellant tank. One of these will be eliminated, since the tankage operation has been tested and the bladder was found to exhibit no restraining force. Thus, in laboratory tests, the only pressure difference observed between the gas and the mercury is due to the mercury head. Latching solenoid valves, requiring power only during open or close operations, had been purchased but were not available for initial tests. Instead, bellows-sealed hand valves were used. Since much of the present work was to prove out initial designs and concepts, components have not been designed for minimum weight. A detailed weight breakdown of the thrustor and propellant tankage systems will be presented with the system description.

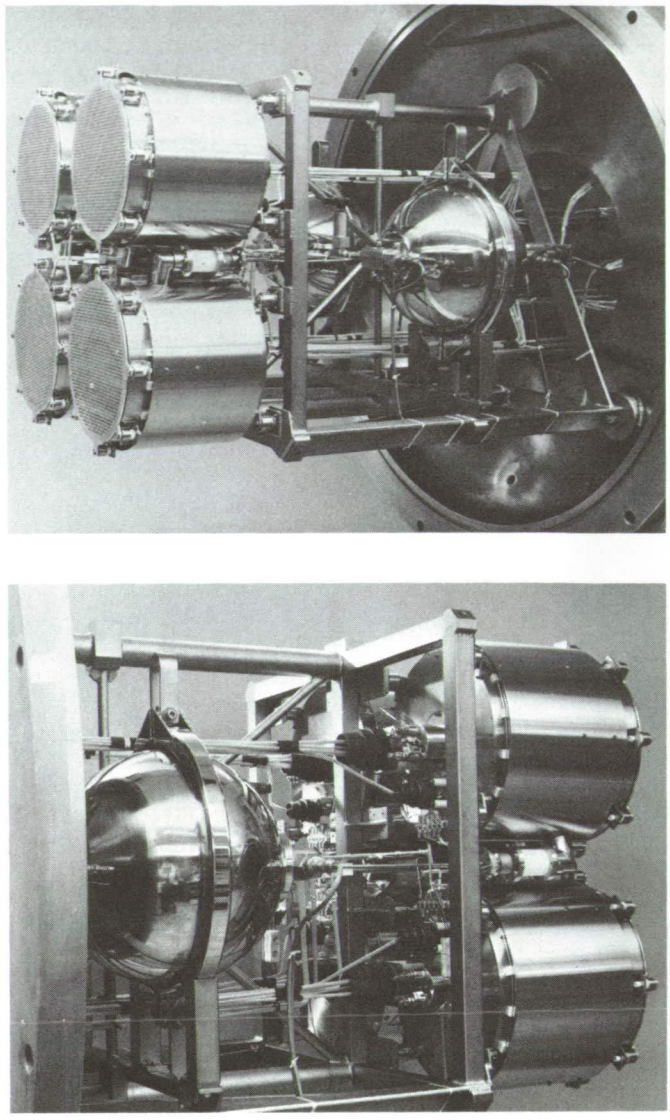

Fig. 4. Thrustor assembly, (a) front view; (b) rear view

E. System Design

The major features of the assembly and the compact thrustor packaging are visible (Figs. 4a and b). All feed lines pass between the thrustors. The smallest thrustor-to-thrustor spacing (0.25 in.) occurs between isolator flanges and a vertically adjacent thrustor. The unheated isolators were all relatively near the thrustors and thus received radiative heating, as well as heating from the vaporizer. A feed-line heater was installed between the isolator and thrustor, but proved to be unnecessary during operation. Thrustors were mounted from four supports using standard alumina insulators. Flatness across thrustors vertically and horizontally, measured without accel grids, was found to be within 0.020 in. without shimming. Standard connectors were used for power and instrumentation wiring. Boron nitride inserts were used in connectors mounted to the thrustors. The use of connectors allowed easy thrustor mounting and removal.

The mounting structure was substantially overdesigned to avoid immediate problems with this component. In addition, the structure will probably be entirely changed for integration with the thrust-vector position control system and extensive design was not warranted. Provisions were made for mounting the 200-lb propellant tanks simply for laboratory use.

The weight breakdown for the assembled system, shown in Figs. 4a and b, is listed by components in Table 2.

Table 2. Present cluster weight breakdown

Component	Weight, lb	
Thrustor (Includes: Feed system to vaporizer, cathode, connector halves, molybdenum grids and neutralizer)	12 (each)	
Total (4 thrustors)		48
Propellant tankage (Includes: 9-in.-diam tank, pressurization system, transducers, valve and feed lines)	14 (each)	
Total (2 tankages)		28
Wiring (to vacuum chamber)		4
Structure		30
Total assembly		110

Table 3. Future cluster weight breakdown

Component	Weight, lb	
Thrustor	9 (each)	
Total (4 thrustors)		36
Propellant tankage (welded titanium construction)	7 (each)	
Total (2 tankages)		14
Wiring		4
Structure		20
Total assembly		74

Estimates for a system designed for lighter weight, but with the same basic design, are given in Table 3. Since the power level is 10 kW, these weights represent 11 and 7.4 lb/kW, respectively. The reduction of about one third to achieve the lighter design appears quite reasonable.

III. System Operation

Preliminary tests of the system were conducted to evaluate component designs and study possible integration problems. Thrustor studies were conducted in the work reported here, and led to substantial improvements over the original design. All tests were performed in a 3-ft × 7-ft vacuum chamber at pressures below 10^{-5} torr. No major difficulty was encountered in single thrustor operation, although chamber cooling was inadequate and full power operation of two or more thrustors was not accomplished. Sputtering was not serious, since long-duration tests were not conducted.

Each of the propellant tanks was filled with approximately 150 lb of mercury. Only a small fraction of this will be used during preliminary testing, but this moderate filling tested the tankage systems, as well as the filling and handling systems and the structure. No basic design problems, such as leaks, loss of pressurization, or failures were encountered. However, a minor difficulty of tankage heating by radiation occurred. This problem was

Table 4. Typical initial thrustor operating conditions[a]

Parameters	Data points				
	1	2	3	4	5
Screen grid voltage, kV	1.40	1.50	1.40	1.50	1.50
Beam current, mA	560	710	655	700	780
Accelerator grid voltage, kV	1.20	1.70	1.50	2.10	2.10
Accelerator current, mA	8.9	5.00	7.6	7.50	8.2
Discharge current, A	12.0	14.5	11.8	12.0	14.0
Discharge voltage, V	32.0	36.5	35.0	35.5	35.5
Cathode current, A	28.0	37.0	35.5	36.5	36.5
Cathode voltage, V	3.15	4.55	4.10	4.10	4.10
Magnet current, A	10.0	12.0	12.0	11.8	12.5
Magnet voltage, V	7.0	8.8	8.8	8.5	9.5
Manifold power, W	4.0	4.0	—	—	—
Vaporizer power, W	3.6	3.6	3.6	3.8	3.8
Propellant flowrate g/h	6.5	6.5	6.5	8.5	8.5
Discharge, eV/ion	686	746	630	608	637
Power efficiency, %	57.8	56.3	57.2	59.8	59.5
Propellant utilization eff., %	64.5	82.0	75.5	61.7	68.8
True specific impulse, s	2420	3170	2830	2385	2660
Test conditions					
Thrustor no.	2	2	2	2	2
Run no.	02	02	02	02	02
Date	7/19/67	7/19/67	7/19/67	7/20/67	7/20/67
Scan no.	1	3	5	3	4
Cathode no.	06	06	06	06	06
Cathode condition[b]	—	—	—	—	—
Length-to-diam ratio	1.0	1.0	1.0	1.0	1.0
Magnet configuration[c]	—	—	—	—	—
Cathode pole piece diam, in.	—	—	—	—	—
Cathode pole piece length, in.	—	—	—	—	—
Screen grid thickness, in.	0.100	0.100	0.100	0.100	0.100
Grid spacing, in.	0.060	0.060	0.060	0.060	0.060

[a]Data represents typical points taken from values plotted in Fig. 5.

[b]Coated with R-500 barium carbonate.

[c] Original, uniform, no. 14 Cu.

solved by replacing the solid ground shield with screen to allow radiation to the cold wall.

A. Thrustor Initial Performance

Performance or efficiency is determined entirely by the thrustor subsystem efficiency. This is because no power is required for operation of the propellant tankage subsystem. The total thrustor efficiency (product of power and propellant utilization efficiencies) obtained during initial tests with the unmodified thrustor is shown in Fig. 5. A curve showing SERT II efficiency (Ref. 5) is plotted (Fig. 5) for reference. A tabulation of typical operating conditions is shown in Table 4. The table shows that the discharge, cathode, and magnet powers are the major thrustor losses. The remainder of the investigation described in this report was aimed at reducing the largest loss, discharge power. Methods for reducing the magnet and cathode powers will be discussed in future reports.

B. Results of Thrustor Modifications

A number of factors, grouped as to major or minor effect, were found to change thrustor efficiency by changing the discharge loss. The major factors were (1) cathode pole piece (a magnetic field shaping iron cylinder), (2) cathode position in the pole piece, and (3) screen grid thickness. The minor factors were (1) propellant flowrate, (2) discharge voltage, (3) total accelerating voltage, (4) magnetic field strength, (5) propellant introduction method, and (6) cathode magnetic field. The effect of each of these was investigated as a function of mass utilization efficiency and will now be discussed in detail. It should be noted that the effects of the major factors, investigated explicitly in this work, were implicit in the SERT II thrustor optimization report (Ref. 20). In addition, many of the minor factors studied here have been observed to some degree in many laboratories, but the explicit effects of these have not been reported.

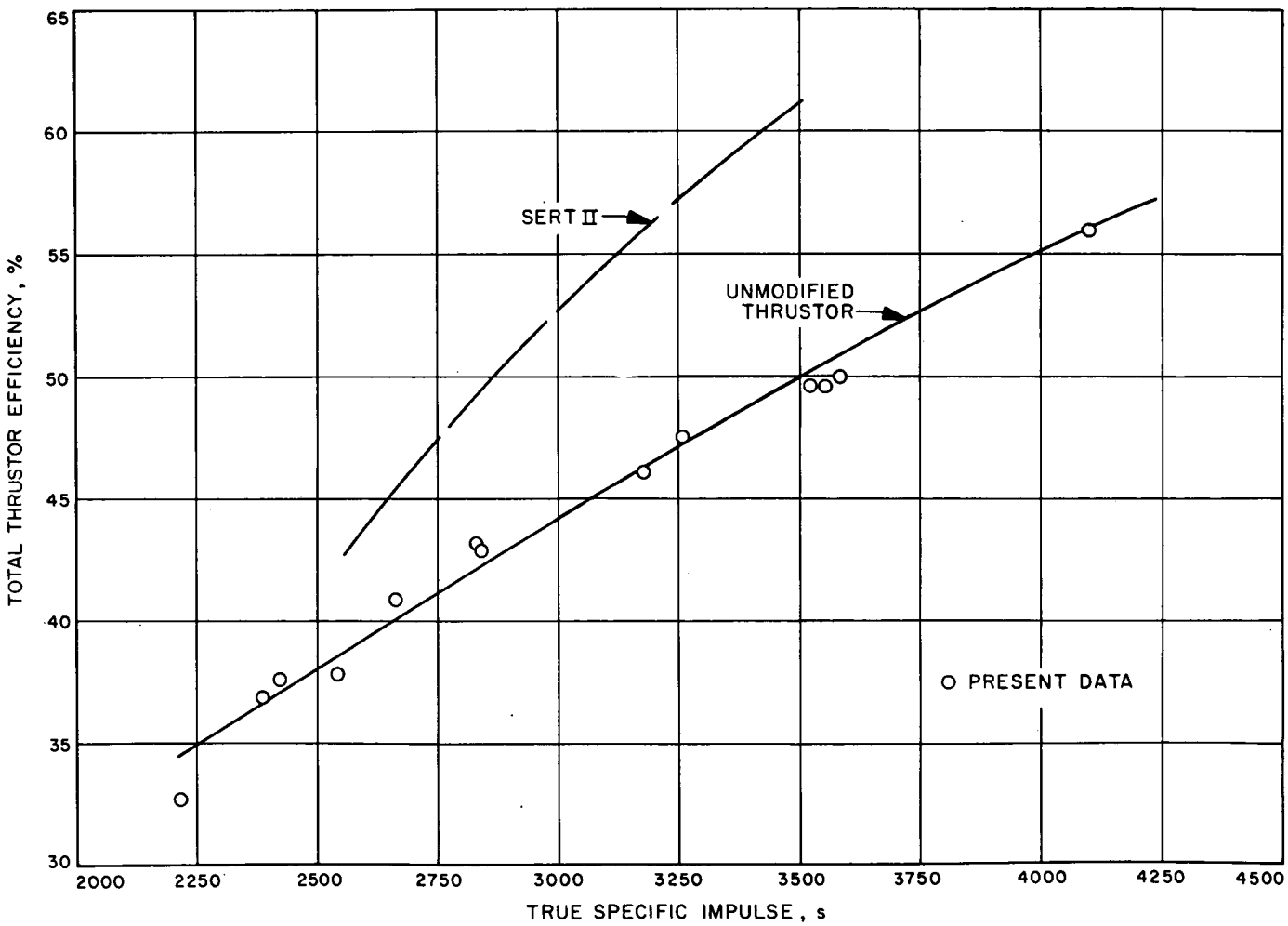

Fig. 5. Initial (unmodified) thrustor total efficiency

The effect of the 3.0-in.-diam cathode pole piece is illustrated in Fig. 6. As indicated on the figure, pole piece lengths of 1.0 and 2.0 in. produced similar results. Thrustor operating conditions are listed in Tables 4 and 5.

Movement of the cathode from the rear of the pole piece to the front, resulted in the improvement shown in Fig. 7. Typical data are listed in Tables 5 and 6. The data of Figs. 6 and 7 were obtained with several propellant flowrates as indicated in the tables. The influence of propellant flowrate, as will be discussed later, was found to significantly shift eV/ion curves and accounts for the scattered appearance of the data on Figs. 6 and 7. With the shifts due to propellant flowrate noted, the data of these figures are relatively consistent.

A further major reduction in the discharge loss was observed by reducing the screen grid thickness. Curves for grid thicknesses of 0.100 and 0.052 in. are presented in Fig. 8. The electromagnet for the engine used in these tests was designed for lower power (double the original number of turns) and to simulate a shortened engine geometry. A comparison of the higher curve of Fig. 8 with the lower curve of Fig. 7 shows both configurations to have similar losses at 75%, but with different curve shapes. The difference between these shapes is not directly apparent, because of the simultaneous length and magnet geometry changes. Data from Fig. 8 are listed in Table 7.

Of the minor factors influencing discharge losses, the propellant flowrate is probably most important. Its importance results from the requirement of power matching in a solar electric system which requires thrustor operation over a 2–to–1 range of flowrates. The changes in discharge losses with changes in propellant flowrate are illustrated in Fig. 9 and are typical for all configurations

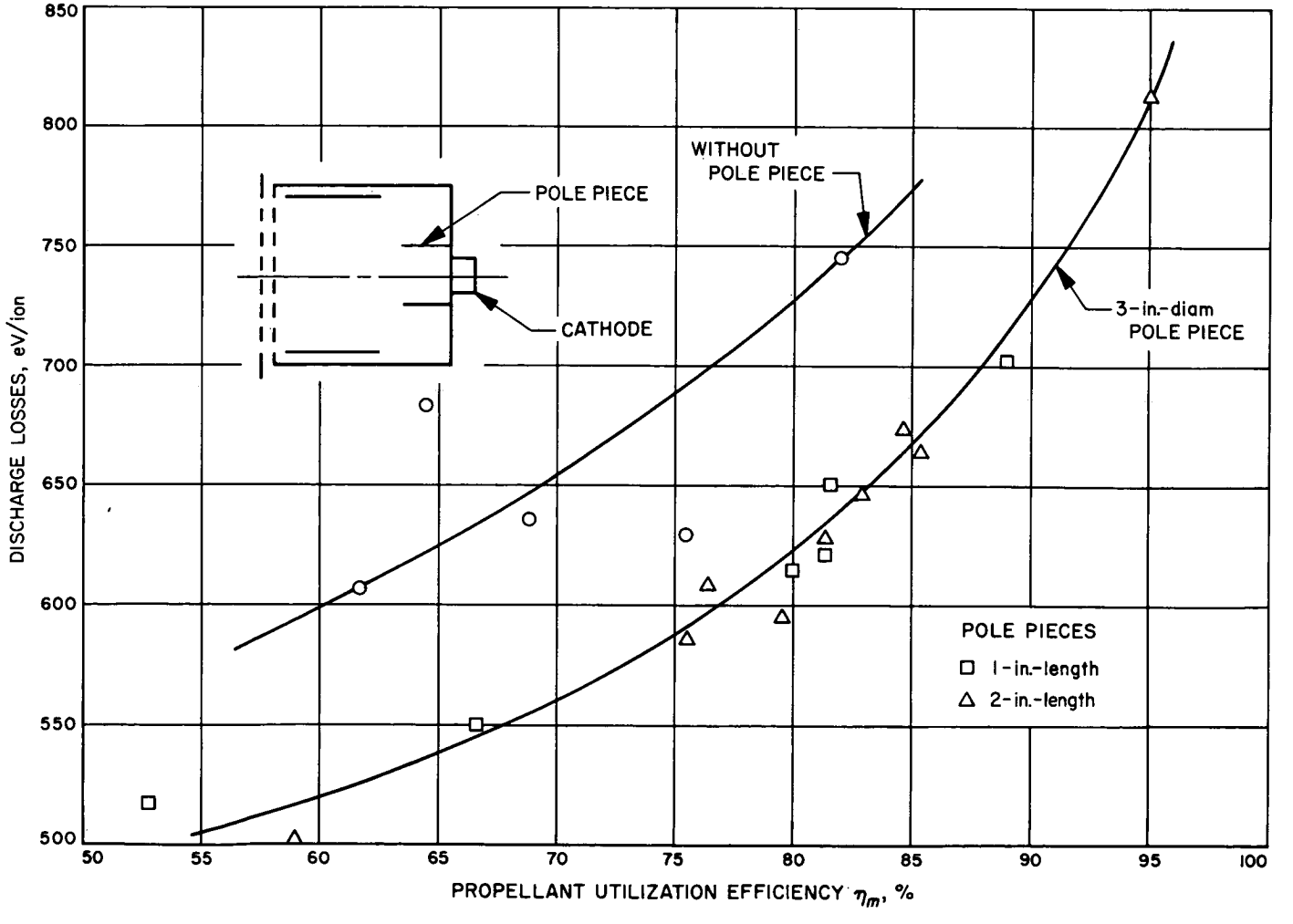

Fig. 6. Effect of cathode pole piece on discharge eV/ion

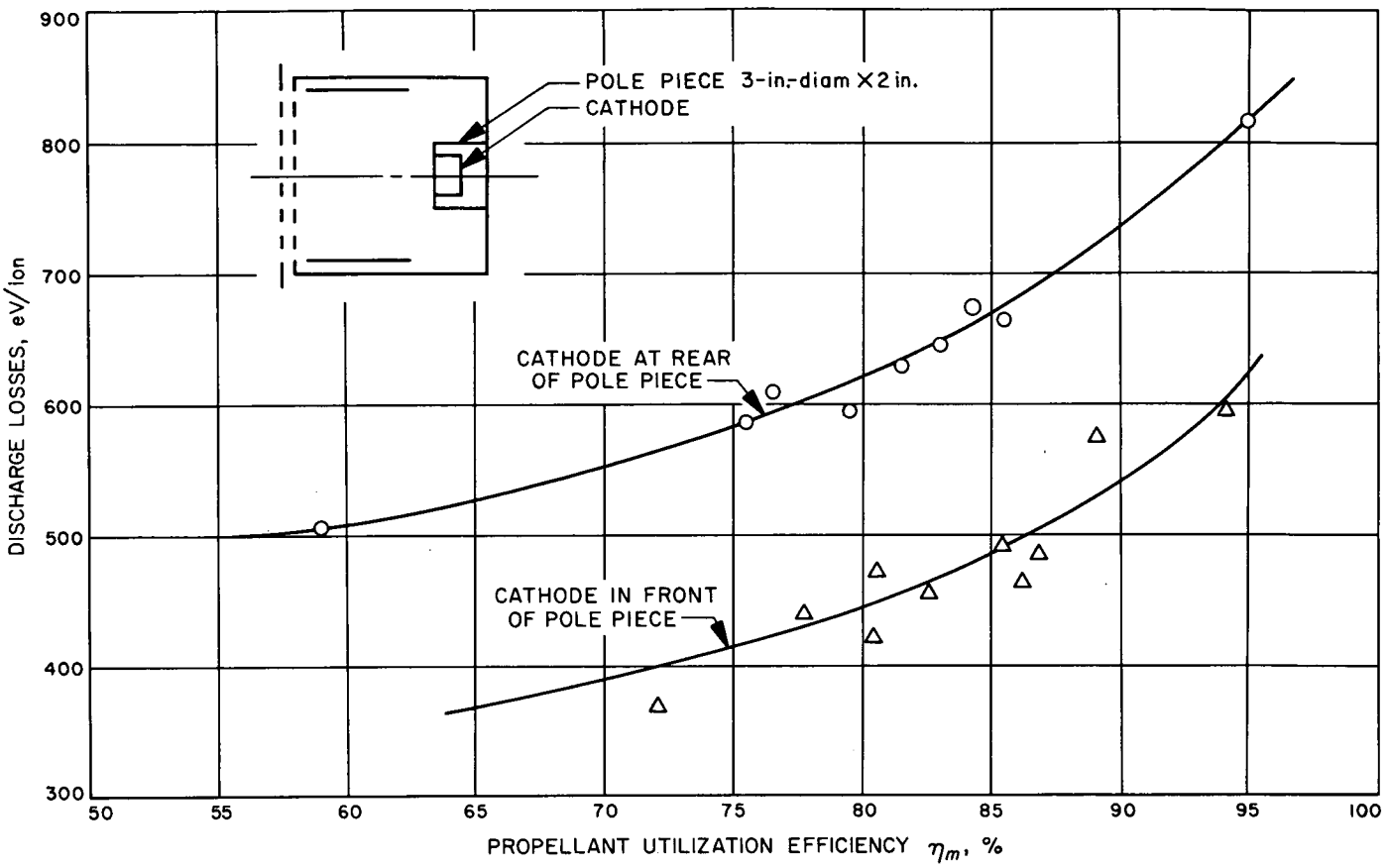

Fig. 7. Effect of cathode position on discharge eV/ion

tested. Operating conditions for some of the data points are given in Tables 7 and 8. It is apparent from this data that comparisons of thrustor configuration or comparisons of operation under different conditions must be performed at the same flowrate.

Discharge voltage was found to influence the discharge loss as shown in Fig. 10. The four voltages produced a consistent trend in which low voltages resulted in lower eV/ion for low mass-utilization efficiency, but produced higher losses at high utilization. The curves cross at approximately 88% utilization, indicating little effect of arc voltage at this point. An additional indication of consistency is that the 32-V curve was obtained during another run at a slightly lower flowrate and was corrected using the previously determined variation of eV/ion with flowrate. Data points in Table 9 show effects of discharge voltage.

The effect of total ion accelerating voltage ($V^+ + |V^-|$) on the discharge is illustrated in Fig. 11 for approximately 1 A of beam current at 81% utilization efficiency. Within the range tested, the discharge eV/ion data are correlated relatively well when plotted against total accelerating voltage, as opposed to plots using V^+ or V^- alone. This is a logical result, since the electric field at the plasma boundary within the thrustor, which affects the shape and area of this boundary, should vary directly with the total accel voltage for constant grid spacing. Data points for these effects are given in Table 10.

The remaining operating parameter, magnetic field strength (Figs. 12 and 13), also significantly affects the discharge. In Fig. 12, the plots of eV/ion against utilization efficiency show the influence of the magnet in reaching high utilization. Figure 13 shows a plot of discharge eV/ion against magnet current at a constant utilization efficiency. Although different thrustors were used to obtain the data in the two figures, the characteristic is similar. The actual magnetic field strengths have not been discussed because these are directly related to the magnet current and would have complicated the previous discussion due to the two-dimensional nature of the field. Typical data used for these figures are listed in Table 11.

Table 5. Effects of 1.0- and 2.0-in. cathode pole piece lengths[a]

Parameters	Data points									
	6	7	8	9	10	11	12	13	14	15
Screen grid voltage, kV	1.90	2.25	2.00	2.00	2.35	1.86	1.86	2.00	2.00	1.90
Beam current, mA	720	810	335	390	500	610	710	565	825	950
Accelerator grid voltage, kV	1.80	2.20	2.00	1.60	2.00	1.35	1.35	1.35	1.70	1.90
Accelerator current, mA	6.2	6.3	2.0	1.2	1.2	4.7	4.3	4.5	9.0	12.0
Discharge current, A	12.3	14.0	5.85	6.7	9.0	12.0	15.0	10.4	15.0	15.0
Discharge voltage, V	36.0	36.0	34.0	38.0	39.0	32.0	38.5	32.0	33.5	41.0
Cathode current, A	43.5	43.5	43.0	41.0	45.0	41.0	41.0	35.0	30.0	21.5
Cathode voltage, V	5.8	5.8	5.7	5.6	6.1	4.95	4.95	4.1	3.65	2.65
Magnet current, A	14.8	14.8	14.9	15.0	14.8	15.0	15.0	15.0	14.8	15.0
Magnet voltage, V	5.8	5.8	5.8	5.9	5.8	5.9	5.9	5.9	5.8	5.9
Manifold power, W	17.2	17.2	17.4	17.4	17.4	17.4	17.4	17.4	14.8	14.8
Vaporizer power, W	1.1	1.4	1.0	1.0	1.0	2.6	2.6	2.6	3.8	4.1
Propellant flowrate, g/h	6.75	7.5	4.0	4.1	4.2	5.6	5.6	5.6	8.1	8.6
Discharge, eV/ion	615	622	561	653	703	630	814	588	610	648
Power efficiency, %	62.5	67.2	56.1	56.7	61.5	61.0	59.0	63.1	68.5	69.2
Propellant utilization eff., %	80.0	81.5	66.3	81.5	89.0	81.5	95.0	75.5	76.5	83.0
True specific impulse, s	3580	3870	2965	3650	4310	3520	4100	3260	3420	3710
Test conditions										
Thrustor no.	4	4	4	4	4	1	1	1	1	1
Run no.	03	03	03	03	03	03	03	03	03	03
Date	8/30/67	8/30/67	8/31/67	8/31/67	8/31/67	8/29/67	8/29/67	8/29/67	8/30/67	8/30/67
Scan no.	7	8	1	2	3	7	8	9	2	3
Cathode no.	08	08	08	08	08	05	05	05	05	05
Cathode condition[b]	—	—	—	—	—	—	—	—	—	—
Length-to-diam ratio	1.0	1.0	1.0	1.0	1.0	1.0	1.0	1.0	1.0	1.0
Magnet configuration[c]	—	—	—	—	—	—	—	—	—	—
Cathode pole piece diam, in.	3.0	3.0	3.0	3.0	3.0	3.0	3.0	3.0	3.0	3.0
Cathode pole piece length, in.	1.0	1.0	1.0	1.0	1.0	2.0	2.0	2.0	2.0	2.0
Screen grid thickness, in.	0.100	0.100	0.100	0.100	0.100	0.100	0.100	0.100	0.100	0.100
Grid spacing, in.	0.070	0.070	0.070	0.070	0.070	0.070	0.070	0.070	0.070	0.070

[a]Data represents typical points taken from values plotted in Fig. 6.

[b]Coated with R-500 barium carbonate.

[c]Uniform, no. 12 Cu.

Table 6. Effects of moving cathode from rear of pole piece to front[a]

Parameters	Data points				
	16	17	18	19	20
Screen grid voltage, kV	1.80	1.80	1.90	1.80	1.80
Beam current, mA	380	520	635	500	600
Accelerator grid voltage, kV	1.40	1.40	1.60	1.60	1.60
Accelerator current, mA	2.25	2.01	4.78	3.42	6.13
Discharge current, A	4.7	8.9	9.7	8.25	8.05
Discharge voltage, V	30.0	40.0	30.0	30.0	33.0
Cathode current, A	36.0	40.0	30.0	36.5	38.0
Cathode voltage, V	4.0	4.9	3.55	4.32	4.5
Magnet current, A	15.0	14.8	14.9	13.2	14.8
Magnet voltage, V	5.1	5.3	5.8	5.1	5.7
Manifold power, W	26.0	26.0	22.5	22.5	23.4
Vaporizer power, W	3.4	3.4	3.5	2.7	3.9
Propellant flowrate, g/h	3.96	3.96	5.77	4.40	5.80
Discharge, eV/ion	371	600	458	495	442
Power efficiency, %	63.1	60.3	69.5	63.7	65.3
Propellant utilization eff., %	72.0	94.0	82.5	85.3	77.6
True specific impulse, s	3060	3990	3600	3620	3300
Test conditions					
Thrustor no.	1	1	1	1	1
Run no.	04	04	04	04	04
Date	9/7/67	9/7/67	9/7/67	9/7/67	9/8/67
Scan no.	1	4	8	10	1
Cathode no.	05	05	05	05	05
Cathode condition[b]	—	—	—	—	—
Length-to-diam ratio	1.0	1.0	1.0	1.0	1.0
Magnet configuration[c]	—	—	—	—	—
Cathode pole piece diam, in.	3.0	3.0	3.0	3.0	3.0
Cathode pole piece length, in.	2.0	2.0	2.0	2.0	2.0
Screen grid thickness, in.	0.100	0.100	0.100	0.100	0.100
Grid spacing, in.	0.070	0.070	0.070	0.070	0.070

[a]Data represents typical points taken from values plotted in Fig. 7.

[b]Coated with R-500 barium carbonate.

[c] Uniform, no. 12 Cu.

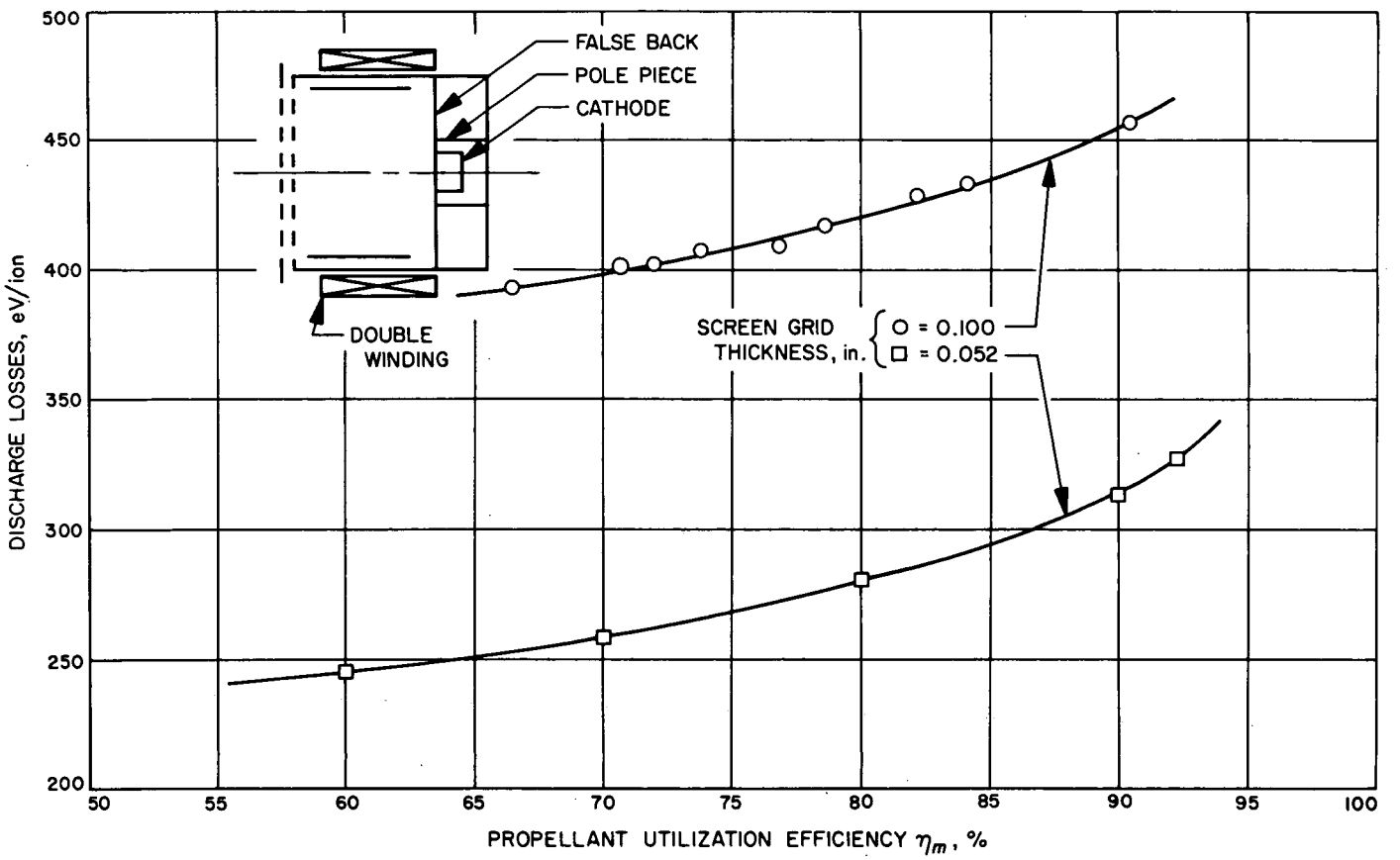

Fig. 8. Effect of screen grid thickness on discharge eV/ion

Table 7. Result of reduced screen grid thickness[a]

Parameters	Data points									
	21	22	23	24	25	26	27	28	29	30
Screen grid voltage, kV	2.00	2.00	2.00	2.00	2.00	2.00	2.00	2.00	2.00	2.00
Beam current, mA	540	600	640	685	735	815	720	615	530	830
Accelerator grid voltage, kV	2.00	2.00	2.00	2.00	2.00	2.00	2.00	2.00	2.00	2.00
Accelerator current, mA	5.80	5.70	5.60	5.60	5.60	5.45	6.40	5.95	6.35	5.45
Discharge current, A	6.10	7.00	7.65	8.50	9.60	7.30	5.80	4.55	3.70	7.80
Discharge voltage, V	35.0	35.0	35.0	35.0	35.0	35.0	35.0	35.0	35.0	35.0
Cathode current, A[b]	—	—	—	—	—	33.5	32.5	32.0	31.0	34.5
Cathode voltage, V[b]	—	—	—	—	—	3.9	3.7	3.5	3.4	4.0
Magnet current, A	9.0	9.0	9.0	9.0	9.0	8.0	8.0	8.0	8.0	8.0
Magnet voltage, V	4.7	4.7	4.7	4.7	4.7	3.7	3.7	3.6	3.6	3.6
Manifold power, W[c]	—	—	—	—	—	—	—	—	—	—
Vaporizer power, W[b]	—	—	—	—	—	3.9	3.9	3.9	3.9	3.9
Propellant flowrate, g/h	6.10	6.10	6.10	6.10	6.10	6.70	6.70	6.70	6.70	6.70
Discharge, eV/ion	395	408	418	434	457	313	282	259	245	329
Power efficiency, %	—	—	—	—	—	78.7	79.0	79.0	78.3	78.0
Propellant utilization eff., %	66.5	73.8	78.6	84.2	90.4	90.0	80.0	70.0	60.0	92.3
True specific impulse, s	2975	3300	3520	3765	4040	4030	3580	3135	2690	4135
Test conditions										
Thrustor no.	3	3	3	3	3	3	3	3	3	3
Run no.	08	08	08	08	08	10	10	10	10	10
Date	10/17/67	10/17/67	10/17/67	10/17/67	10/17/67	10/17/67	10/17/67	10/17/67	10/17/67	10/17/67
Scan no.	—	—	—	—	—	7	8	10	11	12
Cathode no.	07	07	07	07	07	02	02	02	02	02
Cathode condition[d]	—	—	—	—	—	—	—	—	—	—
Length-to-diam ratio	0.72	0.72	0.72	0.72	0.72	0.72	0.72	0.72	0.72	0.72
Magnet configuration[e]	—	—	—	—	—	—	—	—	—	—
Cathode pole piece diam, in.	3.0	3.0	3.0	3.0	3.0	3.0	3.0	3.0	3.0	3.0
Cathode pole piece length, in.	2.0	2.0	2.0	2.0	2.0	2.0	2.0	2.0	2.0	2.0
Screen grid thickness, in.	0.100	0.100	0.100	0.100	0.100	0.052	0.052	0.052	0.052	0.052
Grid spacing, in.	0.070	0.070	0.070	0.070	0.070	0.050	0.050	0.050	0.050	0.050

[a]Data represents typical points taken from values plotted in Figs. 8 and 9.

[b]Parameter not recorded.

[c]Parameter not recorded, except at data points 26–30.

[d]Coated with R-500 barium carbonate, except at data points 26–30, which used a new cathode.

[e]Double winding, no. 12 Cu.

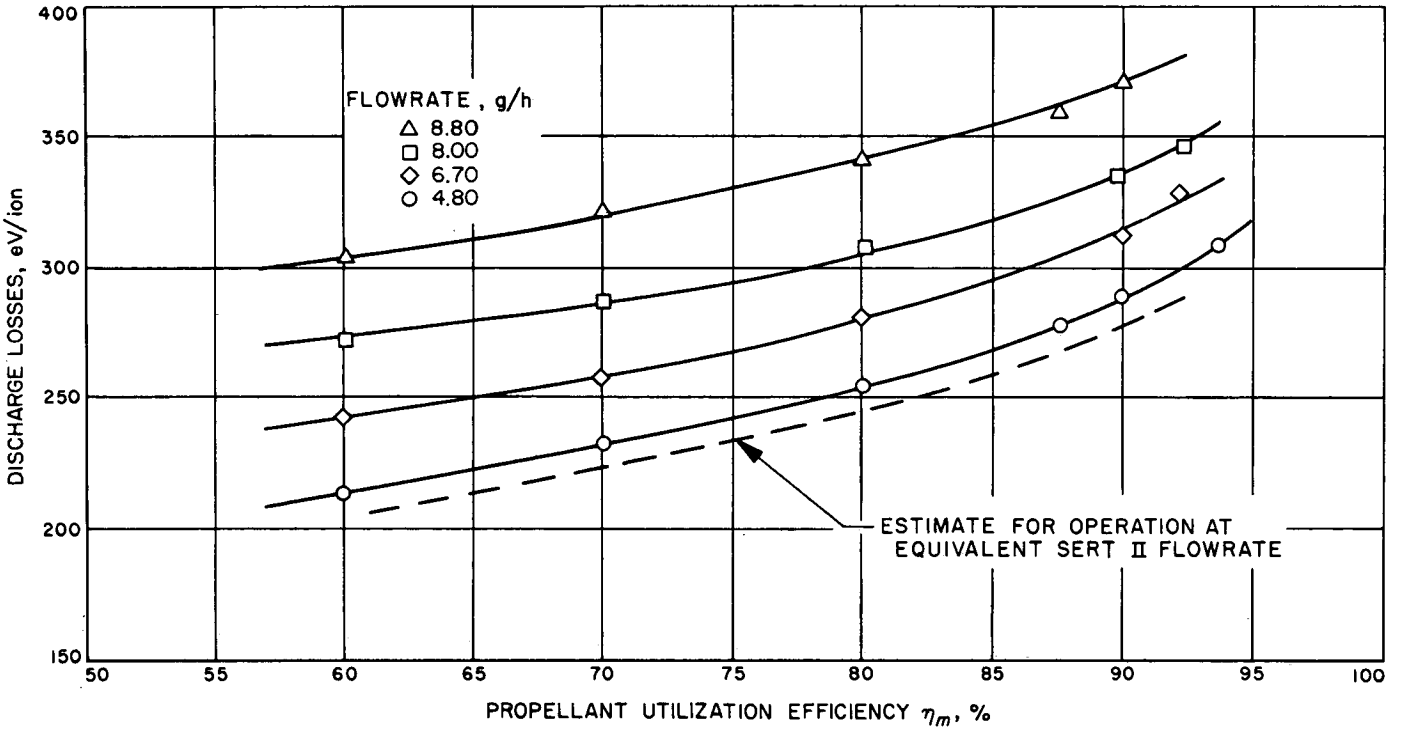

Fig. 9. Effect of propellant flowrate on discharge eV/ion

Table 8. Result of changes in propellant flowrate[a]

Parameters	Data points									
	31	32	33	34	35	36	37	38	39	40
Screen grid voltage, kV	2.00	2.00	2.00	2.00	2.00	2.00	2.00	2.00	2.00	2.00
Beam current, mA	600	575	510	450	385	755	865	960	1,000	640
Accelerator grid voltage, kV	2.00	2.00	2.00	2.00	2.00	2.00	2.00	2.00	2.00	2.00
Accelerator current, mA	2.75	2.90	3.25	3.50	3.70	8.40	7.80	7.30	7.00	8.30
Discharge current, A	5.3	4.75	3.72	3.0	3.35	6.20	7.60	9.20	9.85	5.00
Discharge voltage, V	35.0	35.0	35.0	35.0	35.0	35.0	35.0	35.0	35.0	35.0
Cathode current, A	34.0	33.0	31.0	31.0	30.0	32.0	33.0	33.5	34.0	31.0
Cathode voltage, V	3.9	3.7	3.4	3.3	3.1	3.6	3.8	4.0	4.1	3.4
Magnet current, A	9.0	9.0	9.4	9.0	9.0	7.0	7.0	7.0	7.0	7.0
Magnet voltage, V	4.0	4.0	4.2	4.0	4.0	3.3	3.3	3.3	3.4	3.4
Manifold power, W	—	—	—	—	—	—	—	—	—	—
Vaporizer power, W	3.3	3.3	3.3	3.3	3.3	4.4	4.4	4.4	4.4	4.4
Propellant flowrate, g/h	4.80	4.80	4.80	4.80	4.80	8.00	8.00	8.00	8.00	8.00
Discharge, eV/ion	307	289	255	233	213	287	308	336	345	273
Power efficiency, %	77.6	77.4	78.1	77.5	77.1	79.3	79.8	79.0	78.9	79.5
Propellant utilization eff., %	93.8	90.0	80.0	70.0	60.0	70.0	80.0	90.0	92.3	60.0
True specific impulse, s	4200	4030	3580	3135	2685	3135	3580	4030	4135	2885
Test conditions										
Thrustor no.	3	3	3	3	3	3	3	3	3	3
Run no.	10	10	10	10	10	10	10	10	10	10
Date	11/17/67	11/17/67	11/17/67	11/17/67	11/17/67	11/17/67	11/17/67	11/17/67	11/17/67	11/17/67
Scan no.	1	2	3	4	5	13	14	15	16	17
Cathode no.	02	02	02	02	02	02	02	02	02	02
Cathode condition[b]	—	—	—	—	—	—	—	—	—	—
Length-to-diam ratio	0.72	0.72	0.72	0.72	0.72	0.72	0.72	0.72	0.72	0.72
Magnet configuration[c]	—	—	—	—	—	—	—	—	—	—
Cathode pole piece diam, in.	3.0	3.0	3.0	3.0	3.0	3.0	3.0	3.0	3.0	3.0
Cathode pole piece length, in.	2.0	2.0	2.0	2.0	2.0	2.0	2.0	2.0	2.0	2.0
Screen grid thickness, in.	0.052	0.052	0.052	0.052	0.052	0.052	0.052	0.052	0.052	0.052
Grid spacing, in.	0.050	0.050	0.050	0.050	0.050	0.050	0.050	0.050	0.050	0.050

[a]Data represents typical points taken from values plotted in Fig. 9.

[b]New cathode.

[c]Double winding, no. 12 Cu.

Table 8 (contd)

Parameters	Data points				
	41	42	43	44	45
Screen grid voltage, kV	2.00	2.00	2.00	2.00	2.00
Beam current, mA	1015	1055	940	820	705
Accelerator grid voltage, kV	2.00	2.00	2.00	2.00	2.00
Accelerator current, mA	9.20	9.75	9.60	10.00	10.50
Discharge current, A	10.45	11.20	9.22	7.58	6.15
Discharge voltage, V	35.0	35.0	35.0	35.0	35.0
Cathode current, A	31.0	31.0	29.5	28.0	26.5
Cathode voltage, V	3.6	3.7	3.4	3.1	2.9
Magnet current, A	6.5	6.5	6.5	6.5	6.5
Magnet voltage, V	3.2	3.2	3.2	3.2	3.2
Manifold power, W	—	—	—	—	—
Vaporizer power, W	4.6	4.6	4.6	4.6	4.6
Propellant flowrate, g/h	8.70	8.80	8.80	8.80	8.80
Discharge, eV/ion	360	372	343	323	305
Power efficiency, %	79.0	79.0	79.5	79.8	79.6
Propellant utilization eff., %	87.5	90.0	80.0	70.0	60.0
True specific impulse, s	3915	4030	3580	3135	2685
Test conditions					
Thrustor no.	3	3	3	3	3
Run no.	10	10	10	10	10
Date	11/27/67	11/27/67	11/27/67	11/27/67	11/27/67
Scan no.	1	2	3	4	5
Cathode no.	02	02	02	02	02
Cathode condition[b]	—	—	—	—	—
Length-to-diam ratio	0.72	0.72	0.72	0.72	0.72
Magnet configuration[c]	—	—	—	—	—
Cathode pole piece diam, in.	3.0	3.0	3.0	3.0	3.0
Cathode pole piece length, in.	2.0	2.0	2.0	2.0	2.0
Screen grid thickness, in.	0.052	0.052	0.052	0.052	0.052
Grid spacing, in.	0.050	0.050	0.050	0.050	0.050

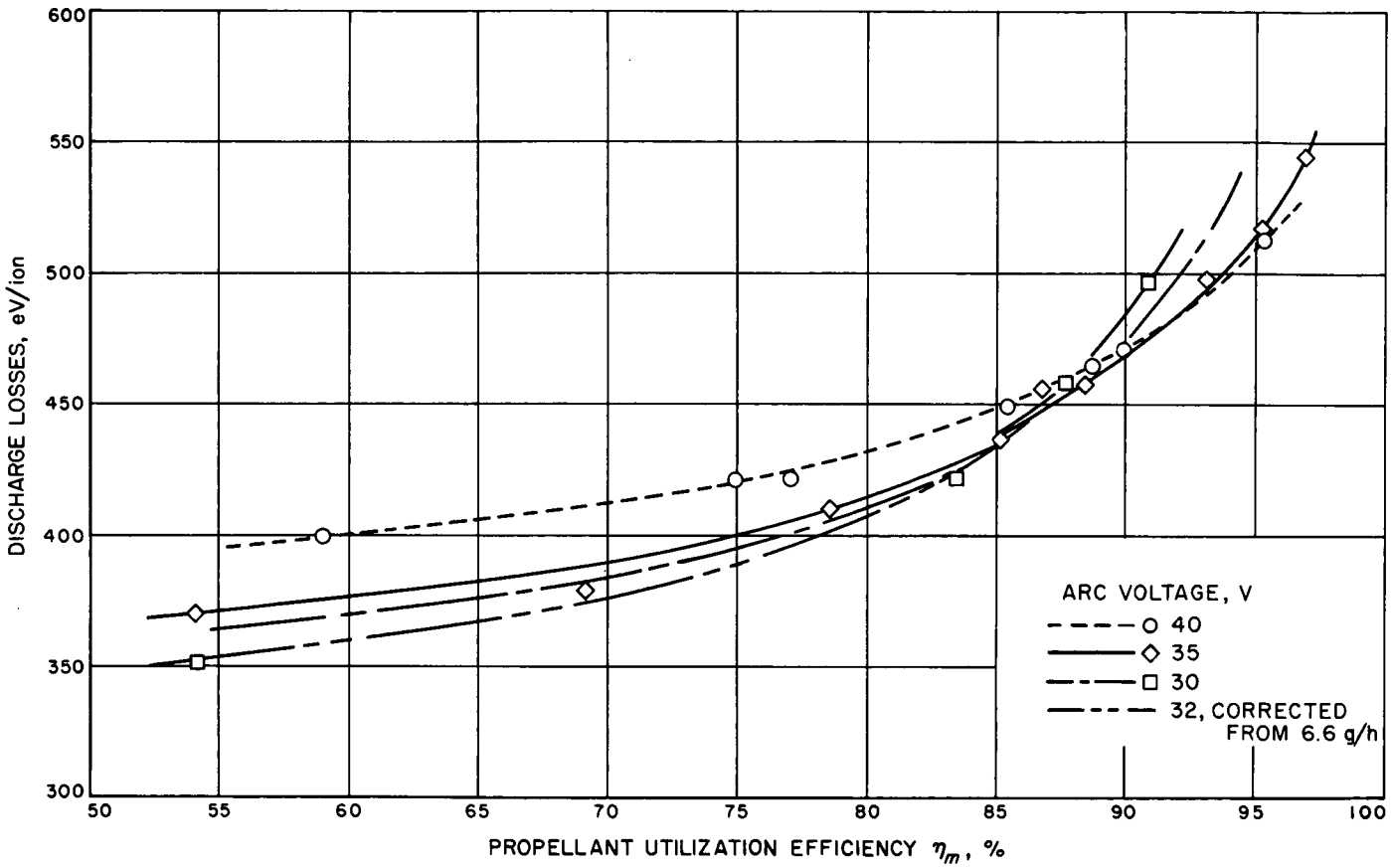

Fig. 10. Effect of arc voltage on discharge eV/ion

Table 9. Effects of discharge voltage[a]

Parameters	Data points									
	46	47	48	49	50	51	52	53	54	55
Screen grid voltage, kV	2.00	2.00	2.00	2.00	2.00	2.00	2.00	2.00	2.00	2.00
Beam current, mA	800	550	840	890	700	795	890	825	735	500
Accelerator grid voltage, kV	2.00	2.00	2.00	2.00	2.00	2.00	2.00	2.00	2.00	2.00
Accelerator current, mA	6.70	7.40	6.90	6.60	7.10	6.60	6.20	6.50	6.80	7.30
Discharge current, A	9.02	5.50	9.93	11.50	7.40	9.92	13.15	10.8	8.6	5.3
Discharge voltage, V	40.0	40.0	40.0	40.0	40.0	35.0	35.0	35.0	35.0	35.0
Cathode current, A	32.0	30.5	33.0	34.0	33.0	34.5	37.0	35.5	35.0	33.0
Cathode voltage, V	3.6	3.3	3.8	4.0	3.6	4.0	4.6	4.3	4.0	3.5
Magnet current, A	15.0	14.9	15.0	15.0	15.0	15.0	15.0	15.0	15.0	14.9
Magnet voltage, V	5.8	5.6	5.7	5.7	5.6	5.7	5.7	5.7	5.8	5.5
Manifold power, W	16.0	16.0	16.0	9.3	9.3	9.3	9.0	9.0	9.0	9.0
Vaporizer power, W	3.1	3.1	3.1	3.1	3.2	3.2	3.2	3.2	3.2	3.2
Propellant flowrate, g/h	7.00	7.00	7.00	7.00	7.00	7.00	7.00	7.00	7.00	7.00
Discharge, eV/ion	452	400	473	517	356	437	518	459	410	371
Power efficiency, %	73.0	71.8	72.6	71.2	72.2	72.3	70.4	71.6	72.4	70.2
Propellant utilization eff., %	85.4	59.0	90.0	95.3	75.0	85.2	95.4	88.4	78.7	53.6
True specific impulse, s	3820	2640	4030	4255	3355	3810	4260	3950	3520	2400
Test conditions										
Thrustor no.	2	2	2	2	2	2	2	2	2	2
Run no.	08	08	08	08	08	08	08	08	08	08
Date	10/16/67	10/16/67	10/16/67	10/16/67	10/16/67	10/16/67	10/16/67	10/16/67	10/16/67	10/16/67
Scan no.	2	4	5	6	16	7	10	12	13	15
Cathode no.	09	09	09	09	09	09	09	09	09	09
Cathode condition[b]	—	—	—	—	—	—	—	—	—	—
Length-to-diam ratio	0.75	0.75	0.75	0.75	0.75	0.75	0.75	0.75	0.75	0.75
Magnet configuration[c]	—	—	—	—	—	—	—	—	—	—
Cathode pole piece diam, in.	3.0	3.0	3.0	3.0	3.0	3.0	3.0	3.0	3.0	3.0
Cathode pole piece length, in.	2.0	2.0	2.0	2.0	2.0	2.0	2.0	2.0	2.0	2.0
Screen grid thickness, in.	0.100	0.100	0.100	0.100	0.100	0.100	0.100	0.100	0.100	0.100
Grid spacing, in.	0.070	0.070	0.070	0.070	0.070	0.070	0.070	0.070	0.070	0.070

[a]Data represents typical points taken from values plotted in Fig. 10.

[b]New cathode.

[c]Uniform, no. 12 Cu.

Table 9 (contd)

Parameters	Data points			
	56	57	58	59
Screen grid voltage, kV	2.00	2.00	2.00	2.00
Beam current, mA	505	780	820	850
Accelerator grid voltage, kV	2.00	2.00	2.00	2.00
Accelerator current, mA	7.4	6.7	6.5	6.4
Discharge current, A	6.0	11.02	12.56	14.2
Discharge voltage, V	30.0	30.0	30.0	30.0
Cathode current, A	35.0	37.0	38.5	41.0
Cathode voltage, V	3.8	4.4	4.7	5.1
Magnet current, A	15.0	15.0	15.0	15.0
Magnet voltage, V	5.6	5.6	5.6	5.6
Manifold power, W	9.0	9.0	9.0	9.0
Vaporizer power, W	3.2	3.2	3.2	3.2
Propellant flowrate, g/h	7.00	7.00	7.00	7.00
Discharge, eV/ion	356	424	460	497
Power efficiency, %	69.9	71.8	70.8	69.3
Propellant utilization eff., %	54.2	83.6	87.8	91.0
True specific impulse, s	2425	3740	3925	4070
Test conditions				
Thrustor no.	2	2	2	2
Run no.	08	08	08	08
Date	10/16/67	10/16/67	10/16/67	10/16/67
Scan no.	17	18	19	20
Cathode no.	09	09	09	09
Cathode condition[b]	—	—	—	—
Length-to-diam ratio	0.75	0.75	0.75	0.75
Magnet configuration[c]	—	—	—	—
Cathode pole piece diam, in.	3.0	3.0	3.0	3.0
Cathode pole piece length, in.	2.0	2.0	2.0	2.0
Screen grid thickness, in.	0.100	0.100	0.100	0.100
Grid spacing, in.	0.070	0.070	0.070	0.070

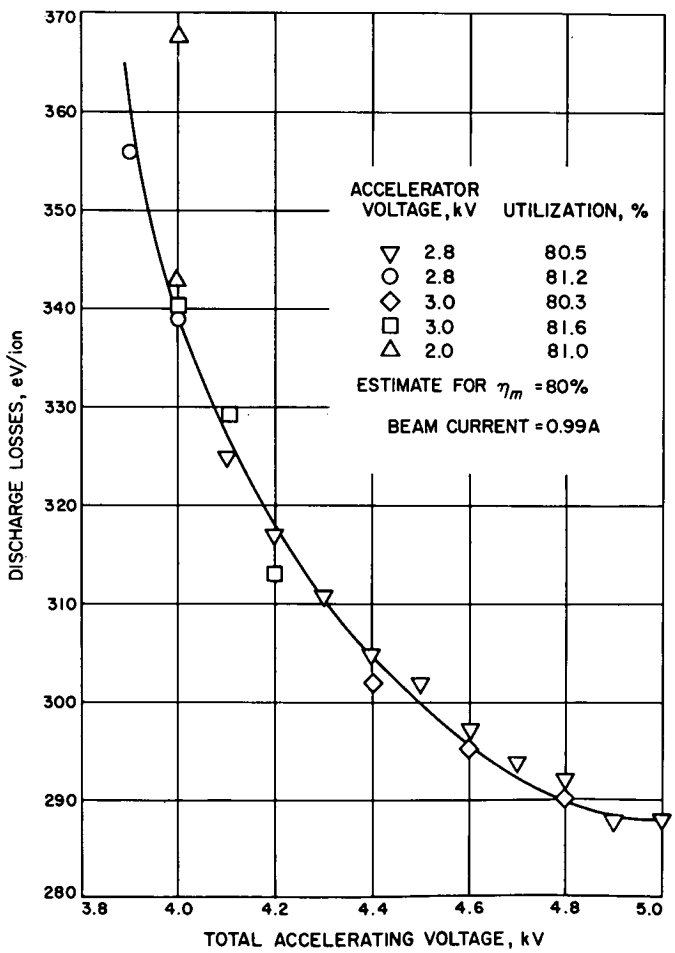

Fig. 11. Effect of total (screen plus accelerator) ion accelerating voltage on discharge eV/ion

Table 10. Effects of total ion accelerating voltage[a]

Parameters	Data points													
	60	61	62	63	64	65	66	67	68	69	70	71	72	73
Screen grid voltage, kV	1.10	1.20	1.40	1.60	1.80	2.00	2.20	1.20	1.40	1.60	1.80	2.00	2.00	2.00
Beam current, mA	990	990	990	990	990	990	990	990	990	990	990	990	940	1000
Accelerator grid voltage, kV	2.80	2.80	2.80	2.80	2.80	2.80	2.80	3.00	3.00	3.00	3.00	3.00	2.00	2.00
Accelerator current, mA	11.10	10.90	10.85	10.65	10.55	10.40	10.20	10.70	10.80	10.65	10.50	10.40	9.60	10.70
Discharge current, A	10.05	9.60	8.95	8.62	8.41	8.26	8.15	8.85	8.55	8.35	8.20	8.15	9.22	10.50
Discharge voltage, V	35.0	35.0	35.0	35.0	35.0	35.0	35.0	35.0	35.0	35.0	35.0	35.0	35.0	35.0
Cathode current, A	32.5	32.0	31.5	31.0	30.5	30.5	30.5	31.0	30.5	30.5	30.5	31.0	29.5	29.0
Cathode voltage, V	3.8	3.7	3.5	3.5	3.5	3.4	3.4	3.5	3.4	3.4	3.4	3.4	3.4	3.4
Magnet current, A	6.25	6.5	7.1	7.6	7.6	7.6	7.6	7.2	7.5	7.8	7.8	7.8	6.5	6.0
Magnet voltage, V	3.0	3.1	3.5	3.7	3.7	3.6	3.6	3.5	3.6	3.7	3.7	3.7	3.2	3.0
Manifold power, W	8.0	8.0	8.0	16.0	4.0	4.0	4.0	8.0	8.0	8.0	8.0	8.0	—	—
Vaporizer power, W	4.8	4.8	4.8	4.8	4.8	4.8	4.8	4.8	4.8	4.8	4.8	4.8	4.4	4.4
Propellant flowrate, g/h	9.15	9.15	9.22	9.22	9.22	9.22	9.22	9.10	9.25	9.25	9.25	9.25	8.80	9.40
Discharge, eV/ion	356	339	317	305	297	292	288	313	302	295	290	288	323	367
Power efficiency, %	66.7	69.2	73.5	76.3	78.8	80.8	82.2	70.7	74.1	77.0	79.0	80.8	79.5	79.0
Propellant utilization eff., %	81.2	81.2	80.5	80.5	80.5	80.5	80.5	81.6	80.3	80.3	80.3	80.3	80.0	79.8
True specific impulse, s	2690	2810	3015	3220	3420	3600	3770	2825	3000	3210	3410	3590	3580	3570
Test conditions														
Thrustor no.	3	3	3	3	3	3	3	3	3	3	3	3	3	3
Run no.	10	10	10	10	10	10	10	10	10	10	10	10	10	10
Date	12/1/67	12/1/67	12/1/67	12/1/67	12/1/67	12/1/67	12/1/67	12/1/67	12/1/67	12/1/67	12/1/67	12/1/67	11/27/67	11/27/67
Scan no.	12	11	9	7	2	4	6	15	16	17	18	19	3	7
Cathode no.	02	02	02	02	02	02	02	02	02	02	02	02	02	02
Cathode condition[b]	—	—	—	—	—	—	—	—	—	—	—	—	—	—
Length-to-diam ratio	0.72	0.72	0.72	0.72	0.72	0.72	0.72	0.72	0.72	0.72	0.72	0.72	0.72	0.72
Magnet configuration[c]	—	—	—	—	—	—	—	—	—	—	—	—	—	—
Cathode pole piece diam, in.	3.0	3.0	3.0	3.0	3.0	3.0	3.0	3.0	3.0	3.0	3.0	3.0	3.0	3.0
Cathode pole piece length, in.	2.0	2.0	2.0	2.0	2.0	2.0	2.0	2.0	2.0	2.0	2.0	2.0	2.0	2.0
Screen grid thickness, in.	0.052	0.052	0.052	0.052	0.052	0.052	0.052	0.052	0.052	0.052	0.052	0.052	0.052	0.052
Grid spacing, in.	0.050	0.050	0.050	0.050	0.050	0.050	0.050	0.050	0.050	0.050	0.050	0.050	0.050	0.050

[a]Data represents typical points taken from values plotted in Fig. 11.

[b]New cathode.

[c]Double winding, no. 12 Cu.

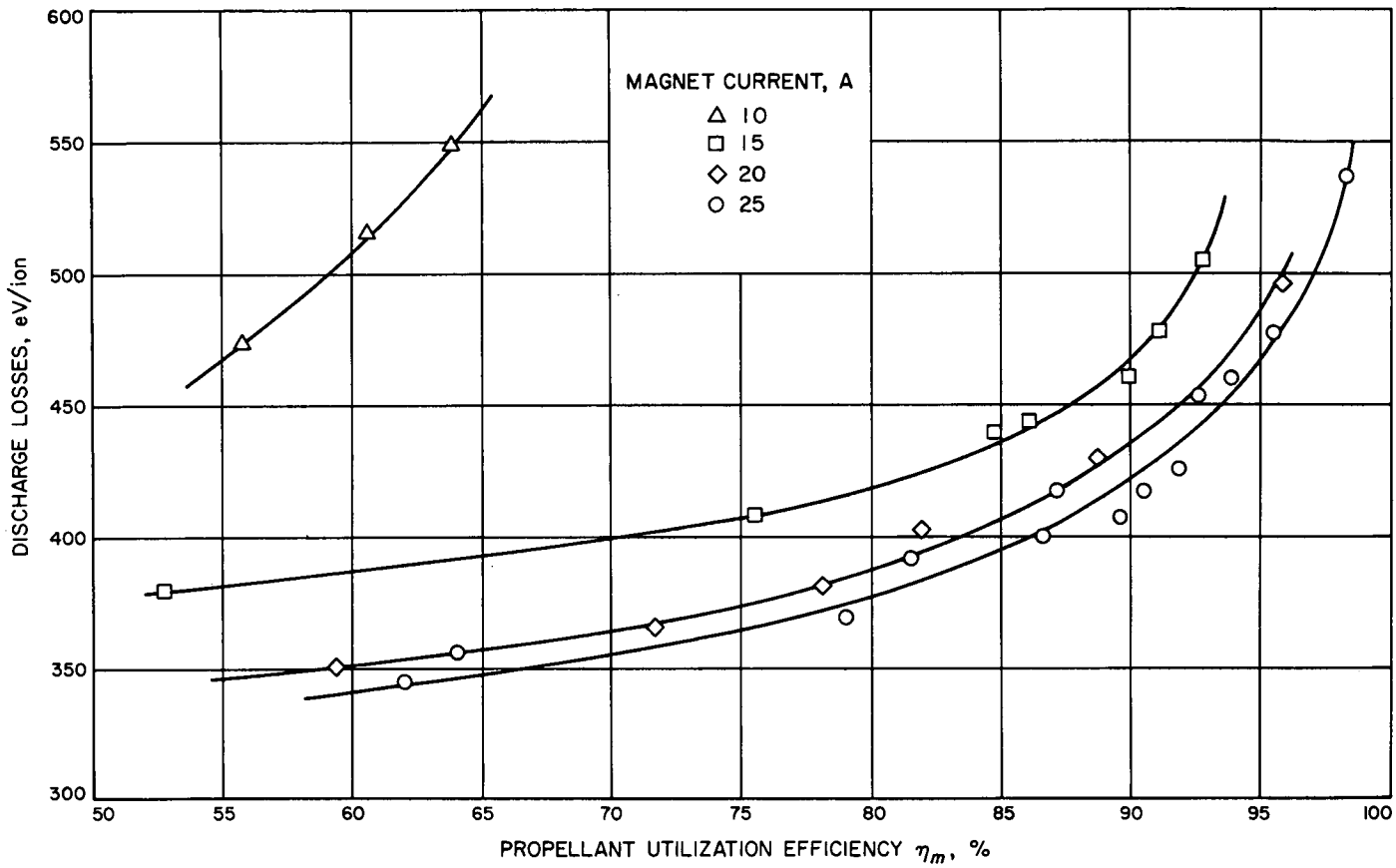

Fig. 12. Effect of magnet current on discharge eV/ion as a function of utilization

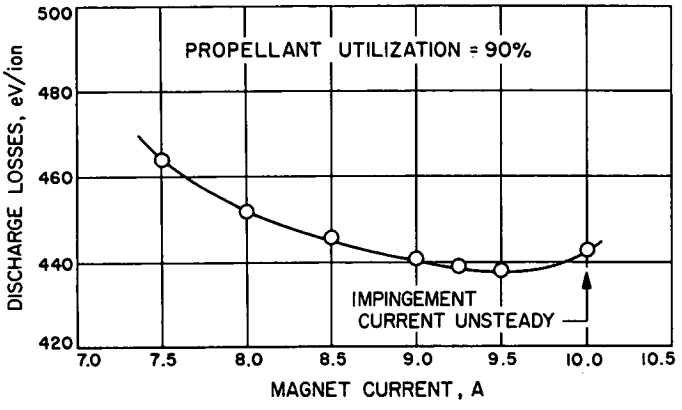

Fig. 13. Effect of magnet current on discharge eV/ion for 90% utilization

Table 11. Effects of magnetic field strength[a]

Parameters	Data points									
	74	75	76	77	78	79	80	81	82	83
Screen grid voltage, kV	2.00	2.00	2.00	2.00	2.00	2.00	2.00	2.00	2.00	2.00
Beam current, mA	465	490	428	405	580	660	710	700	455	605
Accelerator grid voltage, kV	2.00	2.00	2.00	2.00	2.00	2.00	2.00	2.00	2.00	2.00
Accelerator current, mA[b]	—	—	—	—	—	—	—	—	—	—
Discharge current, A	6.85	7.70	5.80	4.40	6.78	8.40	10.25	9.60	4.55	6.60
Discharge voltage, V	35.0	35.0	35.0	35.0	35.0	35.0	35.0	35.0	35.0	35.0
Cathode current, A	40.5	41.0	39.0	35.0	36.5	38.0	42.0	40.5	32.5	34.0
Cathode voltage, V	5.2	5.4	4.9	4.3	4.6	5.0	5.7	5.3	3.9	4.2
Magnet current, A	10.0	10.0	10.0	15.0	15.0	15.0	15.0	15.0	20.0	20.0
Magnet voltage, V	3.7	3.7	3.6	5.9	6.0	6.0	6.1	6.2	8.7	8.6
Manifold power, W[c]	—	—	—	—	—	—	—	—	—	—
Vaporizer power, W[b]	—	—	—	—	—	—	—	—	—	—
Propellant flowrate, g/h	5.75	5.75	5.75	5.75	5.75	5.75	5.75	5.75	5.75	5.75
Discharge, eV/ion	516	550	475	380	409	445	506	480	350	381
Power efficiency, %	—	—	—	—	—	—	—	—	—	—
Propellant utilization eff., %	60.6	63.9	55.8	52.8	75.6	86.1	92.6	91.2	59.4	78.2
True specific impulse, s	2715	2860	2500	2365	3385	3860	4150	4080	2660	3500
Test conditions										
Thrustor no.	1	1	1	1	1	1	1	1	1	1
Run no.	07	07	07	07	07	07	07	07	07	07
Date	10/4/67	10/4/67	10/4/67	10/4/67	10/4/67	10/4/67	10/4/67	10/4/67	10/4/67	10/4/67
Scan no.	—	—	—	—	—	—	—	—	—	—
Cathode no.	06	06	06	06	06	06	06	06	06	06
Cathode condition[d]	—	—	—	—	—	—	—	—	—	—
Length-to-diam ratio	0.75	0.75	0.75	0.75	0.75	0.75	0.75	0.75	0.75	0.75
Magnet configuration[e]	—	—	—	—	—	—	—	—	—	—
Cathode pole piece diam, in.	3.0	3.0	3.0	3.0	3.0	3.0	3.0	3.0	3.0	3.0
Cathode pole piece length, in.	2.0	2.0	2.0	2.0	2.0	2.0	2.0	2.0	2.0	2.0
Screen grid thickness, in.	0.100	0.100	0.100	0.100	0.100	0.100	0.100	0.100	0.100	0.100
Grid spacing, in.	0.070	0.070	0.070	0.070	0.070	0.070	0.070	0.070	0.070	0.070

[a]Data represents typical points taken from values plotted in Figs. 12 and 13.

[b]Parameter not recorded.

[c]Parameters not recorded at data points 81–98.

[d]Coated with R-500 barium carbonate.

[e]Uniform, no. 12 Cu, except at data points 92–98 that are double winding no. 12 Cu.

Table 11 (contd)

Parameters	Data points									
	84	85	86	87	88	89	90	91	92	93
Screen grid voltage, kV	2.00	2.00	2.00	2.00	2.00	2.00	2.00	2.00	2.25	2.25
Beam current, mA	680	710	735	475	665	695	720	732	815	815
Accelerator grid voltage, kV	2.00	2.00	2.00	2.00	2.00	2.00	2.00	2.00	2.00	2.00
Accelerator current, mA[b]	—	—	—	—	—	—	—	—	6.40	6.50
Discharge current, A	8.40	9.20	10.4	4.7	7.60	8.30	9.50	10.00	10.80	10 50
Discharge voltage, V	35.0	35.0	35.0	35.0	35.0	35.0	35.0	35.0	35.0	35.0
Cathode current, A	36.5	37.0	39.0	31.5	32.5	32.5	34.0	34.0	44.0	42.5
Cathode voltage, V	4.7	4.9	5.3	3.8	4.1	4.2	4.5	4.6	5.7	5.4
Magnet current, A	20.0	20.0	20.0	25.0	25.0	25.0	25.0	25.0	7.50	8.00
Magnet voltage, V	9.0	9.0	9.0	11.7	11.7	11.7	11.7	11.7	4.2	4.5
Manifold power, W[c]	—	—	—	—	—	—	—	—	—	—
Vaporizer power, W[b]	—	—	—	—	—	—	—	—	—	—
Propellant flowrate, g/h	5.75	5.75	5.75	5.75	5.75	5.75	5.75	5.75	6.80	6.80
Discharge, eV/ion	432	454	496	346	400	418	462	478	464	452
Power efficiency, %	—	—	—	—	—	—	—	—	—	—
Propellant utilization eff., %	88.7	92.6	95.8	62.0	86.6	90.5	93.8	95.5	90.0	90.0
True specific impulse, s	3970	4150	4290	2775	3880	4050	4200	4270	4270	4270
Test conditions										
Thrustor no.	1	1	1	1	1	1	1	1	3	3
Run no.	07	07	07	07	07	07	07	07	08	08
Date	10/4/67	10/4/67	10/4/67	10/4/67	10/4/67	10/4/67	10/4/67	10/4/67	10/18/67	10/18/67
Scan no.	—	—	—	—	—	—	—	—	—	—
Cathode no.	06	06	06	06	06	06	06	06	07	07
Cathode condition[d]	—	—	—	—	—	—	—	—	—	—
Length-to-diam ratio	0.75	0.75	0.75	0.75	0.75	0.75	0.75	0.75	0.72	0.72
Magnet configuration[e]	—	—	—	—	—	—	—	—	—	—
Cathode pole piece diam, in.	3.0	3.0	3.0	3.0	3.0	3.0	3.0	3.0	3.0	3.0
Cathode pole piece length, in.	2.0	2.0	2.0	2.0	2.0	2.0	2.0	2.0	2.0	2.0
Screen grid thickness, in.	0.100	0.100	0.100	0.100	0.100	0.100	0.100	0.100	0.100	0.100
Grid spacing, in.	0.070	0.070	0.070	0.070	0.070	0.070	0.070	0.070	0.070	0.070

Table 11 (contd)

Parameters	Data points				
	94	95	96	97	98
Screen grid voltage, kV	2.25	2.25	2.25	2.25	2.25
Beam current, mA	815	815	815	815	815
Accelerator grid voltage, kV	2.00	2.00	2.00	2.00	2.00
Accelerator current, mA[b]	6.60	6.70	6.80	7.00	9.00
Discharge current, A	10.35	10.25	10.25	10.20	10.30
Discharge voltage, V	35.0	35.0	35.0	35.0	35.0
Cathode current, A	41.0	41.0	40.5	40.5	40.0
Cathode voltage, V	5.3	5.1	5.1	5.1	5.0
Magnet current, A	8.50	9.00	9.25	9.50	10.0
Magnet voltage, V	4.7	5.0	5.1	5.3	5.6
Manifold power, W[c]	—	—	—	—	—
Vaporizer power, W[b]	—	—	—	—	—
Propellant flowrate, g/h	6.80	6.80	6.80	6.80	6.80
Discharge, eV/ion	446	441	439	438	443
Power efficiency, %	—	—	—	—	—
Propellant utilization eff., %	90.0	90.0	90.0	90.0	90.0
True specific impulse, s	4270	4270	4270	4270	4270
Test conditions					
Thrustor no.	3	3	3	3	3
Run no.	08	08	08	08	08
Date	10/18/67	10/18/67	10/18/67	10/18/67	10/18/67
Scan no.	—	—	—	—	—
Cathode no.	07	07	07	07	07
Cathode condition[d]	—	—	—	—	—
Length-to-diam ratio	0.72	0.72	0.72	0.72	0.72
Magnet configuration[e]	—	—	—	—	—
Cathode pole piece diam, in.	3.0	3.0	3.0	3.0	3.0
Cathode pole piece length, in.	2.0	2.0	2.0	2.0	2.0
Screen grid thickness, in.	0.100	0.100	0.100	0.100	0.100
Grid spacing, in.	0.070	0.070	0.070	0.070	0.070

The propellant introduction method was changed from the original "side-reverse" system (Fig. 2) to a "forward" type, in which the propellant is fed from the rear through a baffle. The effect of changing the introduction method is shown in Fig. 14 together with schematic diagrams of the two schemes. The results of the rear-feed tests produced two basic conclusions. First, the discharge loss is higher for all utilization efficiencies, than for the side-feed case. Second, the difference between the feed methods increases rapidly above 80% utilization. These results are probably due to the fact that in the rear-feed case, a fraction of the propellant apparently on the order of 10% by the shift of the curve in Fig. 14, can flow directly through and out of the thrustor without a collision. In the side feed or any other reverse-feed-type system, neutrals cannot escape directly. Additional data with the rear feed system (Fig. 15) also illustrates the rapid increase in discharge loss with utilization. Data points, showing effects of propellant introduction method, are listed in Tables 12 and 13.

The spiral geometry of the cathode used in this work produced an interesting effect on the discharge. The high heating current (30 to 40A) through the cathode produces a magnetic field aiding or opposing the externally applied field. Figure 15 shows the difference between heating the cathode with ac or dc current and Fig. 16 shows the effect of polarity in heating with dc current. The difference between the two curves in Fig. 16 is about twice the difference in Fig. 15. This is a reasonable result considering that the difference in cathode produced fields in the two cases should be about a factor of two. Data points, showing effects of spiral geometry of the cathode, are listed in Table 13.

Accelerator grid impingement, although not related directly to thrustor performance, influences the operating conditions through the effect of impingement on the life expectancy of the grid. Impingement was found to depend primarily upon utilization efficiency and propellant flowrate, and data is presented in Fig. 17. These data points correspond directly to Fig. 9 (see Tables 7 and 8). Figure 17 implies that thrustor grid life, for a given grid design, can be traded for higher power level (through flowrate) or lower specific impulse (through utilization efficiency). This also illustrates that the maximum power level of a given thrustor with constant specific impulse is limited by accelerator impingement.

It is of interest to show the thrustor efficiency after the discharge loss reductions indicated previously. The total efficiency, representative of tests through run 10 of phase I, is shown in Fig. 18 and corresponding data points are listed in Table 10. The figure indicates that the data were obtained for constant flowrate and constant utilization efficiency. Thus, the screen grid voltage was varied to obtain the variable specific impulse. Curves for SERT II (Ref. 5) and a mercury thrustor projection for 1970 are shown for reference.

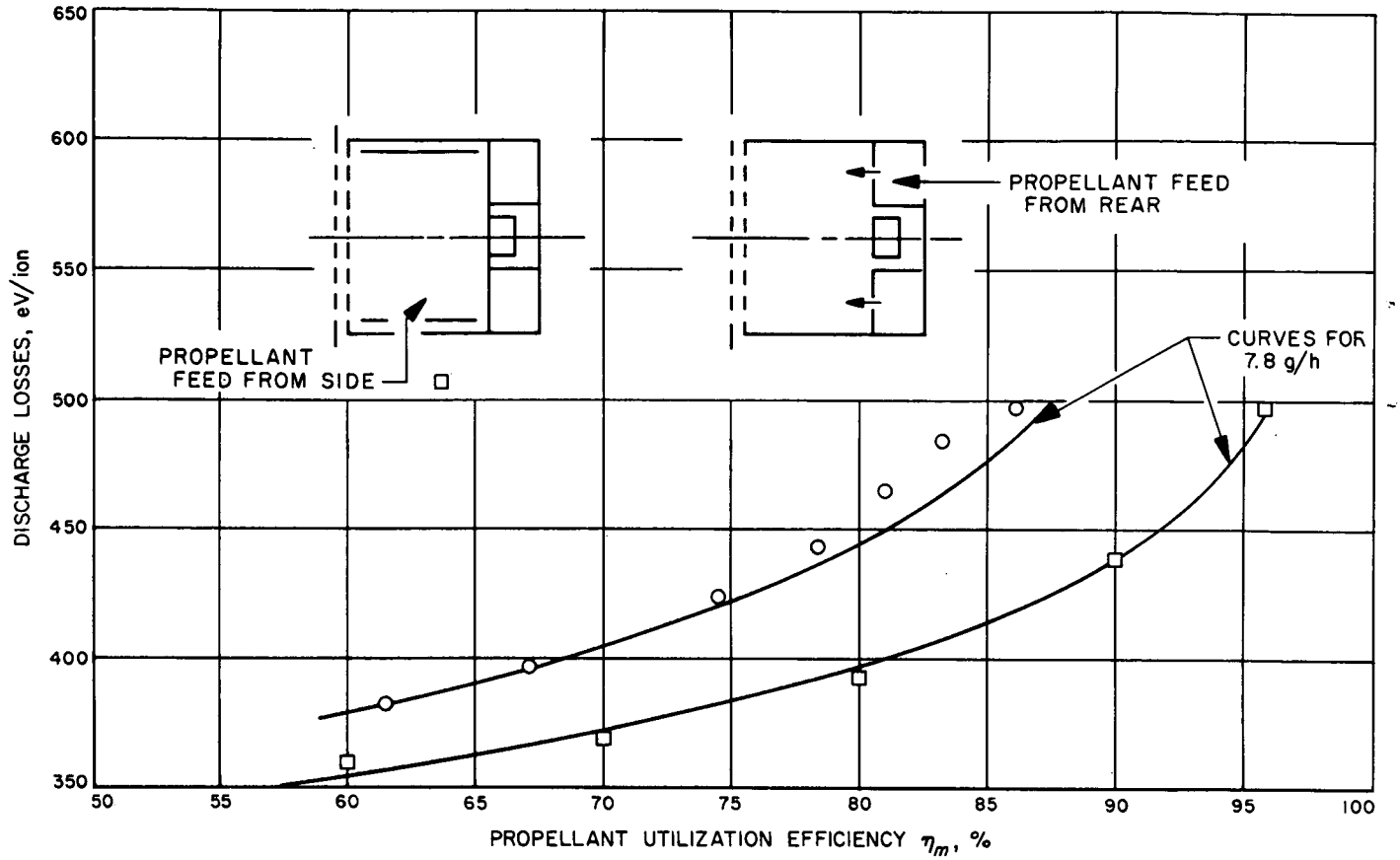

Fig. 14. Effect of propellant introduction method on discharge eV/ion

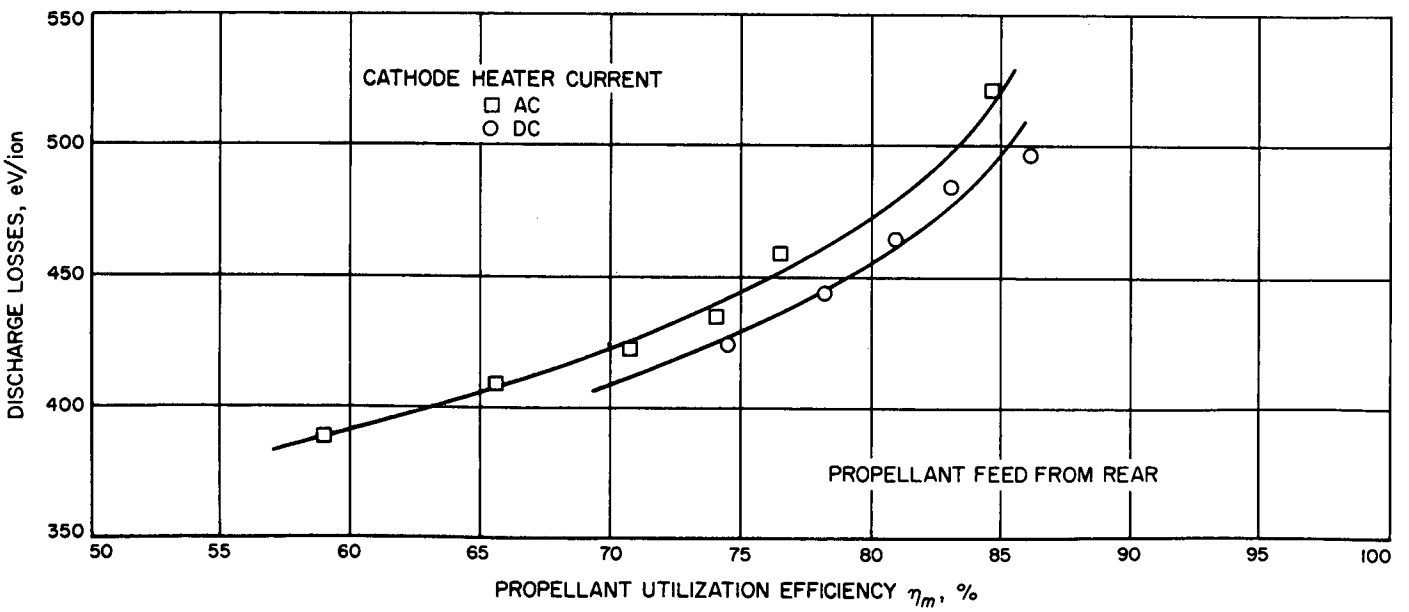

Fig. 15. Effect of ac cathode heater current on discharge eV/ion

Table 12. Effects of propellant introduction method[a]

Parameters	Data points						
	99	100	101	102	103	104	105
Screen grid voltage, kV	2.00	2.00	2.00	2.00	2.00	2.00	2.00
Beam current, mA	935	830	725	620	695	640	795
Accelerator grid voltage, kV	2.00	2.00	2.00	2.00	2.00	2.00	2.00
Accelerator current, mA	8.60	8.80	9.00	9.10	9.00	9.00	8.80
Discharge current, A	11.80	9.40	7.72	6.40	7.80	7.00	9.65
Discharge voltage, V	35.0	35.0	35.0	35.0	35.0	35.0	35.0
Cathode current, A	37.5	36.0	35.0	34.5	30.5	30.5	31.5
Cathode voltage, V	4.2	4.1	3.9	3.7	3.5	3.4	3.8
Magnet current, A	15.0	15.0	15.0	15.0	15.0	15.0	15.0
Magnet voltage, V	5.5	5.5	5.5	5.5	5.4	5.4	5.4
Manifold power, W	9.3	9.3	9.3	9.3	—	—	—
Vaporizer power, W	3.2	3.2	3.2	3.2	4.4	4.4	4.4
Propellant flowrate, g/h	7.80	7.80	7.80	7.80	7.80	7.80	8.00
Discharge, eV/ion	442	396	373	361	392	383	425
Power efficiency, %	72.8	73.3	72.8	72.0	73.5	73.1	73.3
Propellant utilization eff., %	90.0	80.0	70.0	60.0	67.2	61.5	74.5
True specific impulse, s	4030	3580	3135	2685	3010	2755	3330
Test conditions							
Thrustor no.	2	2	2	2	2	2	2
Run no.	08	08	08	08	10	10	10
Date	10/23/67	10/23/67	10/23/67	10/23/67	11/16/67	11/16/67	11/16/67
Scan no.	13	14	15	16	17	18	19
Cathode no.	09	09	09	09	12	12	12
Cathode condition[b]	—	—	—	—	—	—	—
Length-to-diam ratio	0.75	0.75	0.75	0.75	0.75	0.75	0.75
Magnet configuration[c]	—	—	—	—	—	—	—
Cathode pole piece diam, in.	3.0	3.0	3.0	3.0	3.0	3.0	3.0
Cathode pole piece length, in.	2.0	2.0	2.0	2.0	2.0	2.0	2.0
Screen grid thickness, in.	0.100	0.100	0.100	0.100	0.100	0.100	0.100
Grid spacing, in.	0.070	0.070	0.070	0.070	0.070	0.070	0.070

[a]Data represents typical points taken from values plotted in Fig. 14.

[b]Coated with R-500 barium carbonate except cathodes at data points 103 and 104 that were used once, no new coating.

[c]Uniform, no. 12 Cu.

Table 13. Effects of spiral geometry of the cathode[a]

Parameters	Data points									
	106	107	108	109	110	111	112	113	114	115
Screen grid voltage, kV	2.00	2.00	2.00	2.00	2.00	2.00	2.00	2.00	2.00	2.00
Beam current, mA	835	940	885	910	830	765	700	630	905	645
Accelerator grid voltage, kV	2.00	2.00	2.00	2.00	2.00	2.00	2.00	2.00	2.00	2.00
Accelerator current, mA[b]	8.70	8.80	8.70	8.90	—	8.80	8.70	8.70	8.20	6.30
Discharge current, A	10.60	13.35	11.75	12.60	10.90	9.20	8.00	7.00	13.50	8.00
Discharge voltage, V	35.0	35.0	35.0	35.0	35.0	35.0	35.0	35.0	35.0	35.0
Cathode current, A[c]	32.0	33.5	32.5	33.0	38.0	35.5	35.0	34.5	43.0	—
Cathode voltage, V[d]	3.9	4.3	4.1	4.2	4.1	3.8	3.7	3.6	4.8	—
Magnet current, A	15.0	15.0	15.0	15.0	15.0	15.0	15.0	15.0	15.0	15.0
Magnet voltage, V[d]	5.4	5.5	5.4	5.5	5.0	5.3	5.3	5.3	5.3	—
Manifold power, W[e]	—	—	—	—	—	—	—	—	—	—
Vaporizer power, W[b]	4.4	4.4	4.4	4.4	4.4	4.4	4.4	4.4	4.4	—
Propellant flowrate, g/h	8.00	8.20	8.20	8.20	8.10	8.10	8.00	8.00	8.00	6.30
Discharge, eV/ion	444	497	465	485	460	422	411	389	522	434
Power efficiency, %	73.0	71.6	72.8	72.1	71.8	72.6	72.6	72.1	69.4	—
Propellant utilization eff., %	78.3	86.2	81.0	83.1	76.7	70.8	65.6	59.0	84.8	75.0
True specific impulse, s	3500	3860	3625	3720	3435	3170	2940	2640	3790	3355
Test conditions										
Thrustor no.	2	2	2	2	2	2	2	2	2	1
Run no.	10	10	10	10	10	10	10	10	10	08
Date	11/16/67	11/16/67	11/16/67	11/16/67	11/16/67	11/16/67	11/16/67	11/16/67	11/16/67	11/17/67
Scan no.	20	23	21	22	8	11	12	13	14	—
Cathode no.	12	12	12	12	12	12	12	12	12	08
Cathode condition[f]	—	—	—	—	—	—	—	—	—	—
Length-to-diam ratio	0.75	0.75	0.75	0.75	0.75	0.75	0.75	0.75	0.75	0.69
Magnet configuration[g]	—	—	—	—	—	—	—	—	—	—
Cathode pole piece diam, in.	3.0	3.0	3.0	3.0	3.0	3.0	3.0	3.0	3.0	3.5
Cathode pole piece length, in.	2.0	2.0	2.0	2.0	2.0	2.0	2.0	2.0	2.0	2.0
Screen grid thickness, in.	0.100	0.100	0.100	0.100	0.100	0.100	0.100	0.100	0.100	0.100
Grid spacing, in.	0.070	0.070	0.070	0.070	0.070	0.070	0.070	0.070	0.070	0.070

[a]Data represents typical points taken from values plotted in Figs. 14, 15, and 16.

[b]Parameter not recorded.

[c]Alternating current used for data points 110, 111, 113, and 114; parameter not recorded at data points 115–121.

[d]Parameter not recorded.

[e]Parameter not recorded, except at data points 106–114.

[f]Used once, no new coating, except cathodes at data points 116–121 that were coated with R-500 barium carbonate.

[g]Uniform, no. 12 Cu.

Table 13 (contd)

Parameters	Data points					
	116	117	118	119	120	121
Screen grid voltage, kV	2.00	2.00	2.00	2.00	2.00	2.00
Beam current, mA	610	470	590	670	735	790
Accelerator grid voltage, kV	2.00	2.00	2.00	2.00	2.00	2.00
Accelerator current, mA[b]	6.30	6.40	6.30	5.80	5.60	5.60
Discharge current, A	7.30	4.90	6.60	8.00	9.65	11.60
Discharge voltage, V	35.0	35.0	35.0	35.0	35.0	35.0
Cathode current, A[c]	—	—	—	—	—	—
Cathode voltage, V[d]	—	—	—	—	—	—
Magnet current, A	15.0	15.0	15.0	15.0	15.0	15.0
Magnet voltage, V[d]	—	—	—	—	—	—
Manifold power, W[e]	—	—	—	—	—	—
Vaporizer power, W[b]	—	—	—	—	—	—
Propellant flowrate, g/h	6.30	6.30	6.30	6.30	6.30	6.30
Discharge, eV/ion	419	365	392	418	459	514
Power efficiency, %	—	—	—	—	—	—
Propellant utilization eff., %	71.0	56.0	70.2	79.7	87.5	94.0
True specific impulse, s	3180	2505	3140	3560	3915	4200
Test conditions						
Thrustor no.	1	1	1	1	1	1
Run no.	08	08	08	08	08	08
Date	11/17/67	11/17/67	11/17/67	11/17/67	11/17/67	11/17/67
Scan no.	—	—	—	—	—	—
Cathode no.	08	08	08	08	08	08
Cathode condition[f]	—	—	—	—	—	—
Length-to-diam ratio	0.69	0.69	0.69	0.69	0.69	0.69
Magnet configuration[g]	—	—	—	—	—	—
Cathode pole piece diam, in.	3.5	3.5	3.5	3.5	3.5	3.5
Cathode pole piece length, in.	2.0	2.0	2.0	2.0	2.0	2.0
Screen grid thickness, in.	0.100	0.100	0.100	0.100	0.100	0.100
Grid spacing, in.	0.070	0.070	0.070	0.070	0.070	0.070

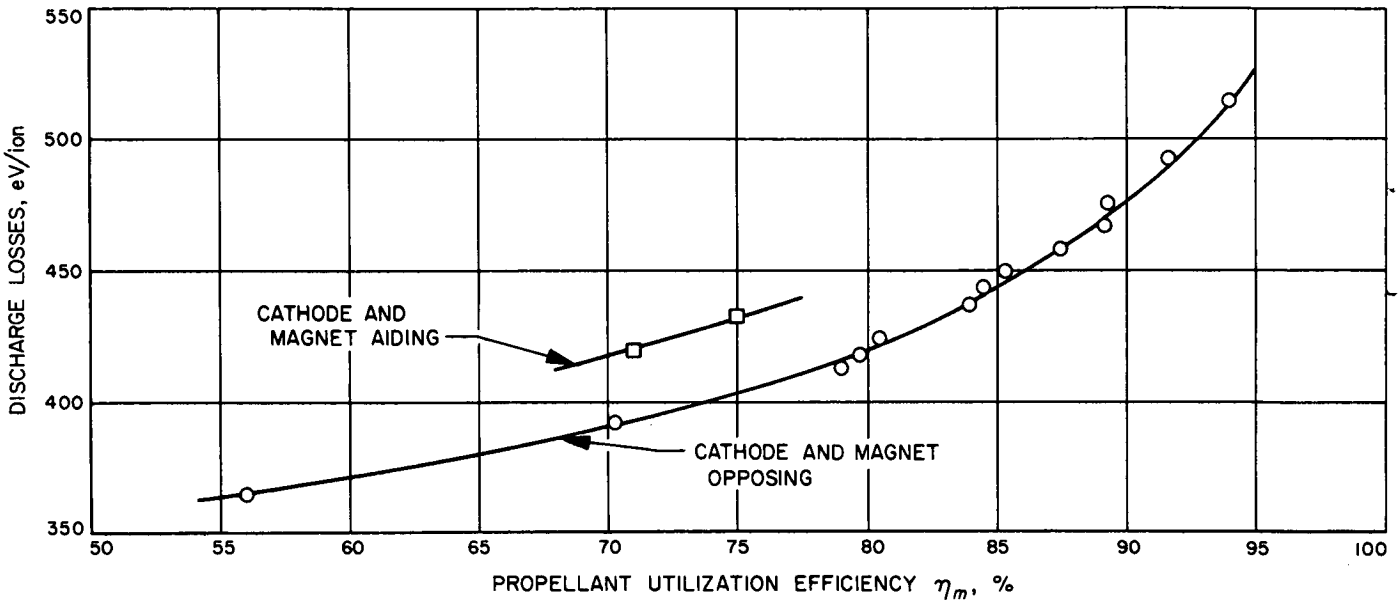

Fig. 16. Effect of dc cathode heater polarity on discharge eV/ion

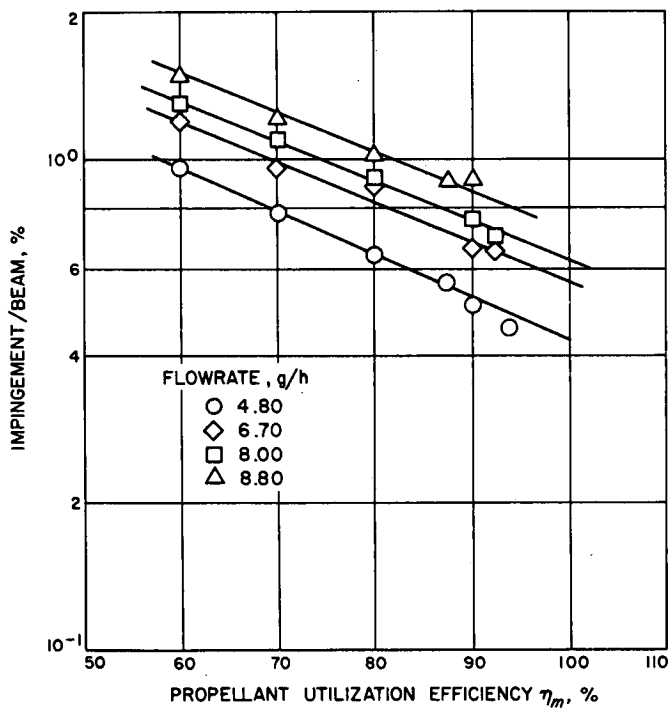

Fig. 17. Effect of propellant flowrate and utilization on impingement current

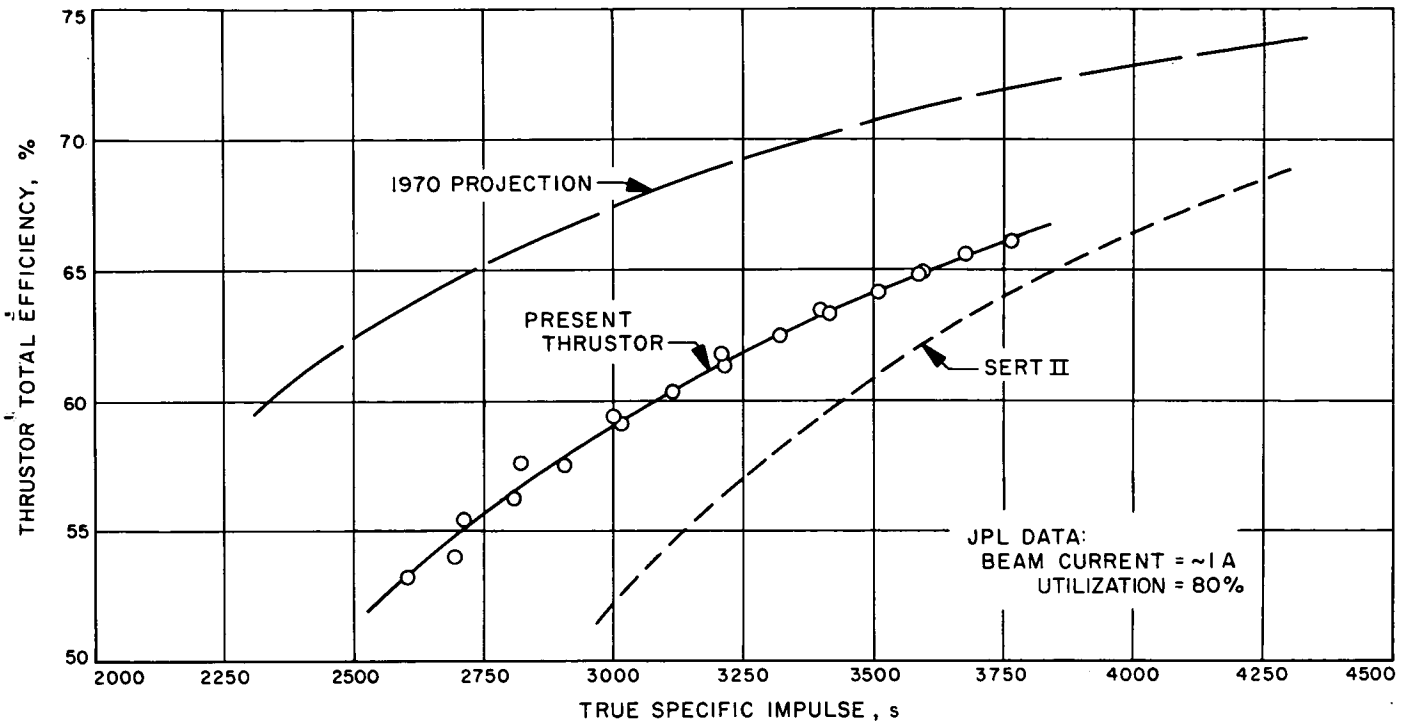

Fig. 18. Present thrustor efficiency for several propellant flowrates

IV. Conclusions

The investigations discussed in this paper justify several conclusions. Thrustor operation was as expected based on previous experience with this type of thrustor. The portions of the thrustor system tested for the first time—closely spaced electrodes, isolators, and vaporizers —performed well and without failure. The completely new propellant tankage system operated as designed, without leaks or loss of pressurization. No difficulties were found in filling or handling the relatively large amounts of mercury. The Freon pressurization design appears to work satisfactorily and Freon should prove to be a convenient lightweight pressurization system. However, a test using a complete tank of propellant should be performed to fully evaluate this system. Integration of the thrustors and propellant tankage systems was accomplished without any serious difficulties. Unfortunately, a four-thrustor test could not be performed because of facility constraints. However, two thrustors were operated simultaneously at about half power with good success. Future tests will include operation with all thrustors at least at low power.

A system efficiency of about 63% at 3500 s was obtained for the 2.5-kW power level. This exceeds the original performance goal and provides confidence that further improvements will be obtained with additional modifications. These modifications will include reduced screen grid thickness, additional magnetic field shaping, smaller (0.147-in.-diam) apertures in both grids, smaller accelerator apertures with 0.187-in.-diam screen apertures and thicker (up to 0.20 in.) accelerator grids. The weight of the existing thrustor and tankage system is only slightly heavier than the initial goal (11 lb/kW compared to 10 lb/kW). This weight can be reduced using demonstrated fabrication techniques and by reducing noncritical part thicknesses.

References

1. *Solar-Powered Electric Propulsion Spacecraft Study*, Report SSD 50094R, Hughes Aircraft Company, Culver City, Calif., Dec. 1965.

2. *Solar-Powered Electric Propulsion Program*, Report SSD 60374, Hughes Aircraft Company, Culver City, Calif., Dec. 1966.

3. Stearns, J. W., and Kerrisk, D. J., "Solar-Powered Electric Propulsion Systems —Engineering and Applications," Paper 66-576, presented at AIAA Second Propulsion Joint Specialists' Conference, Colorado Springs, Colo., June 1966.

4. Ratcheson, W. I., *Fabrication Feasibility of a 20-Watt Per Pound Solar Cell Array*, Technical Report 65-846, Jet Propulsion Laboratory, Pasadena, Calif., Dec. 1965.

5. Kerrisk, D. J., and Kaufman, H. R., "Electric Propulsion Systems For Primary Spacecraft Propulsion," Paper 67-424, presented at AIAA Third Propulsion Joint Specialists' Conference, Washington, D.C., July 1967.

6. Reader, P. D., and Mickelsen, W. R., "Experimental Systems Studies of Large Modules and Arrays of Electrostatic Thrustors," Paper 64-503, presented at First AIAA Annual Meeting, Wash., D.C., June 1964.

7. Stover, J. B., "Effect of Thrustor Arcing on Ion Rocket System Design," Paper 64-682, presented at AIAA Electric Propulsion Specialists' Conference, Phila., Pa., Aug. 1964.

8. Pawlik, E. V., *An Experimental Evaluation of Array of Three Electron Bombardment Ion Thrustors*, NASA TN D-2597. National Aeronautics and Space Administration, Washington, Jan. 1965.

9. Flandro, G. A., and Barber, T. A., "Low Thrust Mission Analysis," Paper 67-678, presented at the AIAA Conference on Electric Propulsion and Plasmadynamics, Colorado Springs, Colo., Sept. 1967.

10. Sauer, C. G., Jr., "Trajectory Analysis and Optimization of a Low-Thrust Solar-Electric Jupiter Flyby Mission," Paper 67-680, presented at the AIAA Conference on Electric Propulsion and Plasmadynamics, Colorado Springs, Colo., Sept. 1967.

11. Reader, P. D., *Experimental Effects of Propellant-Introduction Mode on Electron-Bombardment Ion Rocket Performance*, NASA TN D-2587, Jan. 1965.

12. Reader, P. D., "An Electron Bombardment Ion Rocket With a Permanent Magnet," Paper 63-031, presented at the AIAA Electric Propulsion Specialist Conference, Colorado Springs, Colo., Mar. 1963. (See also *Astronaut and Aerospace Engineering*, Vol. 1, No. 9, p. 83, Oct. 1963.)

13. Sohl, G., Speiser, R. C., and Wolters, J. A., "Life Testing of Electron-Bombardment Cesium Ion Engines," Paper 66-233, presented at the Fifth AIAA Conference on Electric Propulsion, San Diego, Calif., Mar. 1966.

References (contd)

14. Sohl, G., Fosnight, V. V., and Goldner, S. J., *Electron Bombardment Cesium Ion Engine System* (Summary Report on NASA Contract CR-54711), Report 6954, Electro-Optical Systems, Pasadena, Calif., Apr. 1967.

15. Rawlin, V. K., and Pawlik, E. V., "A Mercury Plasma-Bridge Neutralizer," Paper 67-640, presented at the AIAA Conference on Electric Propulsion and Plasmadynamics, Colorado Springs, Colo., Sept. 1967.

16. Klyarfelld, B. N., *Investigations Into Electrical Discharges In Gases*, p. 10, The MacMillan Company, New York, 1964.

17. Santeler, D. J., Holkeboer, D. H., Jones, D. W., and Pagano, F., *Vacuum Technology and Space Simulation*, NASA SP-105, National Aeronautics and Space Administration, Washington, 1966.

18. Kerrisk, D. J., and Masek, T. D., "A Zero-Gravity Mercury Propellant Feed System," Paper 66-250, presented at the Fifth AIAA Conference on Electric Propulsion, San Diego, Calif., Mar. 1966.

19. Bird, R. B., Stewart, W. E., and Lightfoot, E. N., *Transport Phenomena*, pp. 196–200, John Wiley and Sons, Inc., New York, 1960.

20. Bechtel, R. T., "Discharge Chamber Optimization of the SERT II Thrustor," Paper 67-668, presented at the AIAA Conference on Electric Propulsion and Plasmadynamics, Colorado Springs, Colo., Sept. 1967.